

# Confirmation of mass-independent Ni isotopic variability in iron meteorites

Robert C.J. Steele<sup>a,b,\*</sup>, Tim Elliott<sup>a</sup>, Christopher D. Coath<sup>a</sup>, Marcel Regelous<sup>a,c</sup>

<sup>a</sup> Bristol Isotope Group, School of Earth Sciences, University of Bristol, Wills Memorial Building, Queen's Road, Bristol BS8 1RJ, UK

<sup>b</sup> Meteoritics and Cosmic Mineralogy, The Natural History Museum, Cromwell Road, London SW7 5BD, UK

<sup>c</sup> GeoZentrum Nordbayern, Universität Erlangen-Nürnberg, Schlossgarten 5, D-91054 Erlangen, Germany

Received 2 June 2010; accepted in revised form 3 August 2011; available online 28 August 2011

## Abstract

We report high-precision analyses of internally-normalised Ni isotope ratios in 12 bulk iron meteorites. Our measurements of  $^{60}\text{Ni}/^{61}\text{Ni}$ ,  $^{62}\text{Ni}/^{61}\text{Ni}$  and  $^{64}\text{Ni}/^{61}\text{Ni}$  normalised to  $^{58}\text{Ni}/^{61}\text{Ni}$  and expressed in parts per ten thousand (‰) relative to NIST SRM 986 as  $\epsilon^{60}\text{Ni}_{61}^{\text{SS}}$ ,  $\epsilon^{62}\text{Ni}_{61}^{\text{SS}}$  and  $\epsilon^{64}\text{Ni}_{61}^{\text{SS}}$ , vary by 0.146, 0.228 and 0.687, respectively. The precision on a typical analysis is 0.03‰, 0.05‰ and 0.08‰ for  $\epsilon^{60}\text{Ni}_{61}^{\text{SS}}$ ,  $\epsilon^{62}\text{Ni}_{61}^{\text{SS}}$  and  $\epsilon^{64}\text{Ni}_{61}^{\text{SS}}$ , respectively, which is comparable to our sample reproducibility. We show that this ‘mass-independent’ Ni isotope variability cannot be ascribed to interferences, inaccurate correction of instrumental or natural mass-dependent fractionation, fractionation controlled by nuclear field shift effects, nor the influence of cosmic ray spallation. These results thus document the presence of mass-independent Ni isotopic heterogeneity in bulk meteoritic samples, as previously proposed by Regelous et al. (2008) (EPSL 272, 330–338), but our new analyses are more precise and include determination of  $^{64}\text{Ni}$ . Intriguingly, we find that terrestrial materials do not yield homogenous internally-normalised Ni isotope compositions, which, as pointed out by Young et al. (2002) (GCA 66, 1095–1104), may be the expected result of using the exponential (kinetic) law and atomic masses to normalise all fractionation processes. The certified Ni isotope reference material NIST SRM 986 defines zero in this study, while appropriate ratios for the bulk silicate Earth are given by the peridotites JP-1 and DTS-2 and, relative to NIST SRM 986, yield deviations in  $\epsilon^{60}\text{Ni}_{61}^{\text{SS}}$ ,  $\epsilon^{62}\text{Ni}_{61}^{\text{SS}}$  and  $\epsilon^{64}\text{Ni}_{61}^{\text{SS}}$  of  $-0.006\text{‰}$ ,  $0.036\text{‰}$  and  $0.119\text{‰}$ , respectively. There is a strong positive correlation between  $\epsilon^{64}\text{Ni}_{61}^{\text{SS}}$  and  $\epsilon^{62}\text{Ni}_{61}^{\text{SS}}$  in iron meteorites analyses, with a slope of  $3.03 \pm 0.71$ . The variations of Ni isotope anomalies in iron meteorites are consistent with heterogeneous distribution of a nucleosynthetic component from a type Ia supernova into the proto-solar nebula.

© 2011 Elsevier Ltd. All rights reserved.

## 1. INTRODUCTION

The Solar System is comprised of material from a range of chemically and isotopically distinct stellar sources. Investigation of the isotopic compositions between different groups of meteorites can help identify their constituent components and be used to explore how they mixed in the early Solar Sys-

tem. However, many processes, such as those that occurred in the early Solar System, can fractionate nuclides proportionally to their mass differences and so may have altered the isotope ratios from those created by nucleosynthesis. It is possible to remove the effects of these ‘mass-dependent’ processes, while simultaneously correcting for fractionation in the mass spectrometer, by ‘internally normalising’ using a second isotope ratio. Variations in these resulting ‘mass-independent’ isotopic signatures, yield clearer information about the nucleosynthetic heritage of the materials that comprise the Solar System (e.g. Reynolds and Turner, 1964).

For a number of refractory or moderately refractory elements, isotopic ‘anomalies’, or mass-independent isotopic

\* Corresponding author at: Bristol Isotope Group, School of Earth Sciences, University of Bristol, Wills Memorial Building, Queen's Road, Bristol BS8 1RJ, UK. Tel.: +44 0 117 33 15141; fax: +44 0 117 92 53385.

E-mail address: [r.steele@bristol.ac.uk](mailto:r.steele@bristol.ac.uk) (R.C.J. Steele).

deviations from a terrestrial baseline, were found in refractory inclusions during the 1970s and 1980s (e.g. Wasserburg et al., 1977; Lee et al., 1978; McCulloch and Wasserburg, 1978a,b; Papanastassiou and Wasserburg, 1978; Heydegger et al., 1979; Niederer et al., 1980; Birck and Allègre, 1984; Birck and Lugmair, 1988). Even larger anomalies were subsequently found in rare micron-scale presolar grains (e.g. Lewis et al., 1987). Understanding how these and other components were mixed to shape the composition of meteorites requires analyses of bulk samples. Although mass-independent isotopic variations in bulk meteorite samples were first documented for Ti by Niemeier and Lugmair (1984), only more recently have data been obtained for a wider range of elements. This has, in part, been a consequence of advances in mass-spectrometry that make it possible to detect the much smaller isotopic anomalies present in bulk samples.

Nickel isotope cosmochemistry offers some attractive characteristics for the study of meteorites and the early Solar System. As an iron peak element which shows moderately siderophile, moderately refractory behaviour, Ni is sufficiently abundant in most meteorite groups (normally at wt.% concentrations) to make high precision analyses possible. Therefore, an advantage of Ni over lithophile elements, e.g. Ba, Cr or Ti, is that it can be used to compare the isotopic compositions of chondrites, irons and other differentiated meteorites to infer possible genetic relationships. Nickel has five stable isotopes  $^{58}\text{Ni}$ ,  $^{60}\text{Ni}$ ,  $^{61}\text{Ni}$ ,  $^{62}\text{Ni}$  and  $^{64}\text{Ni}$ , in abundances 68.1%, 26.2%, 1.14%, 3.63% and 0.93%, respectively (Gramlich et al., 1989b), which are produced by several nucleosynthetic processes. Of particular interest are the two heaviest isotopes,  $^{62}\text{Ni}$  and  $^{64}\text{Ni}$ , which are thought to be significantly overproduced, relative to the other Ni isotopes, in neutron-rich type Ia supernovae (SN Ia), along with neutron-rich isotopes of other elements, e.g.  $^{54}\text{Cr}$  and  $^{50}\text{Ti}$  (e.g. Nomoto, 1982; Hartmann et al., 1985). Given that anomalies have been previously documented for  $^{54}\text{Cr}$  and  $^{50}\text{Ti}$  in bulk samples (Niemeier and Lugmair, 1984; Rotaru et al., 1992), it might be anticipated that anomalies should exist for  $^{62}\text{Ni}$  and  $^{64}\text{Ni}$ , and that they should be correlated. The Ni system offers the advantage over the Cr and Ti systems of the possibility of correlated neutron-rich anomalies, potentially allowing more detailed investigation of the nucleosynthetic source environment. Theoretical nucleosynthetic modelling (e.g. Nomoto et al., 1997; Woosley, 1997; Rauscher et al., 2002) predicts larger anomalies in  $^{64}\text{Ni}$  than the other Ni isotopes; measurements of refractory inclusions are in keeping with this (Birck and Lugmair, 1988). In addition to these mass-independent non-radiogenic stable isotope variations,  $^{60}\text{Ni}$  has a possible input from  $^{60}\text{Fe}$  with a half-life of  $2.62 \pm 0.04$  Ma (Rugel et al., 2009), which is of interest as a possible heat source for planetary melting and as an early Solar System chronometer.

Measurement of Ni isotopes present significant analytical challenges because of the wide range of relative abundances and the presence of isobaric interferences from Fe, Zn and argide molecules. Perhaps not surprisingly there have been disparities between recent Ni isotope studies (Cook et al., 2006; Quitté et al., 2006; Bizzarro et al.,

2007; Dauphas et al., 2008; Regelous et al., 2008; Chen et al., 2009). Further problems exist for the measurement of  $^{64}\text{Ni}$ , the least abundant Ni isotope, which also suffers a significant isobaric interference from  $^{64}\text{Zn}$ . Although the separation of Zn from Ni is straightforward, Zn is a ubiquitous contaminant both from reagents and labware. While some studies have reported accurate  $^{64}\text{Ni}$  data (e.g. Birck and Lugmair, 1988; Dauphas et al., 2008), several recent studies have been unable to reduce the Zn interference sufficiently during analysis and thus could not report  $^{64}\text{Ni}$  data (e.g. Quitté et al., 2006; Regelous et al., 2008; Chen et al., 2009), indicating that measurement of  $^{64}\text{Ni}$  continues to be a significant analytical challenge.

In this contribution we present a new analytical procedure which allows precise measurement of  $^{64}\text{Ni}$  and explore in some detail the controls on the accuracy relative to the normalising standard of Ni isotope ratios in an attempt to resolve the existing controversy and to allow Ni isotope measurements to place more robust constraints on mixing processes and sources in the early Solar System. The role of sample heterogeneity and incomplete dissolution in generating isotopic variability has been invoked in accounting for divergent mass-independent anomalies in several elements, e.g. Ba, from bulk analyses of chondritic meteorites (Hidaka et al., 2003; Ranen and Jacobsen, 2006; Andreasen and Sharma, 2007; Carlson et al., 2007). Although these considerations should be less important for Ni, see Regelous et al. (2008), we wish to focus on analytical issues and so avoid this additional concern by examining iron meteorites, in which pre-solar signatures should have been efficiently homogenised by magmatic processes during planetesimal differentiation. Admittedly, previous studies suggested mass-independent variations between iron meteorites and sulphide inclusions (Quitté et al., 2006), however these have been refuted by later studies Chen et al. (2009).

## 2. MATERIALS AND METHODS

### 2.1. Terrestrial samples and reference materials

There are seven different terrestrial materials used during this study. They are employed for different purposes and are not all presented in every diagram. NIST SRM 986 (Gramlich et al., 1989a,b) is a highly purified Ni isotopic standard, certified to  $\sim 3\text{‰}$  ( $\sim 7\text{‰}$  for  $^{64}\text{Ni}/^{60}\text{Ni}$ ) by Gramlich et al. (1989a,b), and has been used as the reference for both mass-dependent and mass-independent analyses as in many previous studies (Birck and Allègre, 1984; Cook et al., 2006; Dauphas et al., 2008; Regelous et al., 2008; Chen et al., 2009). NIST SRM 361 is a steel standard, which we use as a terrestrial standard to approximate the matrix of iron meteorites. JP-1 (Imai et al., 1995) is a peridotite which we employ to approximate the matrix of silicate meteorites (chondrites). DTS-2 is a dunite USGS geochemical reference material. Like JP-1 it is a Ni rich sample of Earth's mantle; natural materials that should reasonably represent the bulk silicate Earth (BSE). PtYG is a Ni rich massive sulphide from Agnew, Leinster, Western Australia, kindly sent to us by Martin Gole (BHP Billiton). Models of such Ni ore formation suggest that, while the Ni

is mantle derived, these ores may segregate as a result of interaction between the host magma and the continental crust (Dowling and Hill, 1998), thus they may not retain pristine mantle signatures. CPI Ni ICP-MS concentration standard is a highly purified Ni standard of certified concentration (1000 ppm Ni), which we have used both to determine concentrations and as an additional solution standard for mass-dependent and mass-independent analyses. The final standard is a Sigma NiCl<sub>2</sub>·6H<sub>2</sub>O Salt Lot 53H3487 (hereafter NiSalt) which was used to investigate the influence of mass-dependent fractionation in mass-independent anomalies. NIST SRM 986, CPI and the NiSalt have been processed through the full chemistry and produce identical results when unprocessed (NIST SRM 986) or only processed through a Zn cleanup column (CPI and NiSalt).

## 2.2. Nomenclature

There is a lack of systematic nomenclature able to describe and distinguish the increasing variety of isotope ratio data currently being published. The literature contains confusing use of the same notation for different purposes and different notations used for the same purpose. In the case of elements such as Ni, which have more than four stable isotopes, there is more than one choice of normalising pair. Bizzarro et al. (2007) and Regelous et al. (2008) used the <sup>58</sup>Ni/<sup>61</sup>Ni normalising pair, while other studies (e.g. Cook et al., 2006; Dauphas et al., 2008; Chen et al., 2009) have dominantly used <sup>58</sup>Ni/<sup>62</sup>Ni. In meteorite studies, where there is the possibility of anomalies on all isotopes, the expression of the anomalies is dependent on the choice of the normalising isotope pair. While the differently normalised ratios are easily interconverted, where complete isotopic data are reported (e.g. McCulloch and Wasserburg, 1978a), it must first be clear which isotopes have been used for normalisation. Furthermore, Bizzarro et al. (2007) introduced  $\epsilon^{60}\text{Ni}^*$  to denote <sup>60</sup>Ni anomalies inferred to derive from excesses or deficits from <sup>60</sup>Fe. Since the calculation of  $\epsilon^{60}\text{Ni}^*$  is the same as  $\epsilon^{60}\text{Ni}$  in other work, the addition of the \* is a point of interpretation only.

We adopt a more transparent nomenclature which includes the normalising ratio as a subscript, e.g.  $\epsilon^{60}\text{Ni}_{\text{Ni}^{58/61}}$ . The Ni isotope ratios used in this study are expressed in our proposed notation in Eq. (1).

$$\epsilon^i\text{Ni}_{\text{Ni}^{58/61}} = \left( \frac{\left( \frac{{}^i\text{Ni}/{}^{61}\text{Ni}_{\text{Ni}^{58/61}}}{\text{spl}} \right) - 1}{\left( \frac{{}^i\text{Ni}/{}^{61}\text{Ni}_{\text{Ni}^{58/61}}}{\text{std}} \right)} \right) \times 10^4 \quad (1)$$

where <sup>i</sup>Ni is <sup>60</sup>Ni, <sup>62</sup>Ni or <sup>64</sup>Ni, *spl* is the sample, *std* is the standard and both ratios on the right-hand side are internally normalised to <sup>58</sup>Ni/<sup>61</sup>Ni. Unless otherwise stated, the denominator of the normalising isotope ratio is the denominator of the normalised ratios, i.e. <sup>61</sup>Ni in this case.

Mass-dependent ratios are presented using the standard  $\delta$  notation without the subscript:

$$\delta^{60/58}\text{Ni} = \left( \frac{\left( \frac{{}^{60}\text{Ni}/{}^{58}\text{Ni}_{\text{Ni}}}{\text{spl}} \right) - 1}{\left( \frac{{}^{60}\text{Ni}/{}^{58}\text{Ni}_{\text{Ni}}}{\text{std}} \right)} \right) \times 10^3 \quad (2)$$

For both mass-dependent and mass-independent data it must be noted to which standard the differences are relative in this case, NIST SRM 986.

## 2.3. Chemical separation

### 2.3.1. Dissolution

Iron meteorite samples (~10–20 mg) were leached for 10 min in 0.5 M HCl to remove surficial contamination, then washed twice in acetone and 18.2 MΩ cm water. Typically 90–95% of the sample remained after leaching. Samples were then digested in 6 M HCl overnight at 150 °C, dried down, taken up in 7 M HNO<sub>3</sub> heated and ultrasonicated until fully in solution. Silicate samples (~50–100 mg) were heated for 2 days at 150 °C in 2:1 mixture of 15.4 M HNO<sub>3</sub> and 29 M HF, with several ultrasonication steps. Samples were then dried down and redissolved in 7 M HNO<sub>3</sub>, heated and ultrasonicated until fully in solution. The subsequent chemical purification procedure of Ni builds on that of Regelous et al. (2008).

### 2.3.2. First column: AG50W-X4

This column separates Ni from >95% of the matrix of silicate and iron samples (Wahlgren et al., 1970; Victor, 1986). Samples were dried down, redissolved in 6 M HCl and diluted with acetone in a 1:9 ratio by volume to produce a nominally 0.6 M HCl acetone mixture (hereafter referred to as 6 M HCl:90% acetone solution).

These solutions were loaded onto pre-cleaned Biorad polypropylene columns with a 3 mL resin bed (aspect ratio 7.5:1), filled with Biorad AG50W-X4 200–400 mesh resin. Immediately before loading, the columns were conditioned with 6 M HCl:90% acetone solution. It is important at this stage to fully equilibrate the resin with the HCl acetone mixture in order to avoid the appearance of bubbles after loading the samples. This was achieved by backwashing the HCl acetone mixture through the column, ensuring all the resin was in suspension and could resettle.

The matrices of the meteorites eluted during this first stage are collected so that other isotope systems could be analysed on the same aliquots if required. After loading the sample, two 1 mL aliquots of the 6 M HCl:90% acetone solution are added to ensure that all of the Ni and matrix of the sample is washed into the resin bed. The columns are now washed three times with 10 mL of 6 M HCl:90% acetone solution. Elements eluted in this stage include Fe, Cu and Zn (Strelow et al., 1971). Further elution of matrix elements was achieved with 10 mL of an HCl:acetone solution made by diluting 12 M HCl with acetone in a 1:19 ratio by volume (hereafter referred to as 12 M HCl:95% acetone solution).

To finish, Ni was selectively eluted by passing through a mixture of 5% (by volume) 12 M HCl and 95% 0.1 M dimethylglyoxime (DMG) in acetone solution (hereafter referred to as 12 M HCl:95% 0.1 M DMG acetone solution). DMG is highly soluble in acetone and very readily forms an acetone soluble complex with Ni (Tschugaeff, 1905; Godycki et al., 1953). Nickel elution commences with 1 mL of 12 M HCl:95% 0.1 M DMG acetone. Three 3 mL aliquots of 12 M HCl:95% 0.1 M DMG acetone solution

are then collected. This complexes all the Ni in the column and does not remove significant amounts of matrix elements that remain, including, Mg, Ti, K, Na, Ca, Cr and Al. Finally, beakers are exchanged to collect the rest of the matrix during cleaning, for analysis of other elements if required. The columns were cleaned with two passes each of 18.2 M $\Omega$  cm water and 6 M HCl to wash off any remaining matrix elements.

To prepare for the next stage of chemistry, ~0.5–1 mL of 15.4 M HNO<sub>3</sub> was added to the beakers containing the Ni cut, which were then dried on a hot plate at 90 °C overnight. After this dry down the samples were treated with 15.4 M HNO<sub>3</sub> and 30% H<sub>2</sub>O<sub>2</sub> multiple times, coupled with steps of heating and ultra-sonication, until all the DMG had broken down. This reaction is characterised by a change from a white fluffy residue to a small black or brown spot and, once it has finished, a translucent green spot. The first column was performed twice in order to achieve complete separation of Cr, Ca and Mg from Ni. Separation of these elements is important for chondritic meteorites and for consistency all samples, including the iron meteorites in this study, were treated identically.

### 2.3.3. Second column: TruSpec

This column removes any remaining Fe to blank levels and is of special importance for the iron meteorites in this study. The Fe/Ni of the analytical solutions must be minimised because of the <sup>58</sup>Fe interference on <sup>58</sup>Ni. Also removed by this column are Ti and V. The columns used were shrink fit Teflon, with a 150  $\mu$ L resin volume filled with Eichrom TruSpec resin. The columns were refilled with new resin after three uses. The columns were pre-cleaned with two passes of 0.5 mL of 18.2 M $\Omega$  cm water and then conditioned with two passes of 0.5 mL 7 M HNO<sub>3</sub>. After breaking down any residual DMG (Section 2.3.2) the samples were dissolved in 0.5–1 mL of 7 M HNO<sub>3</sub>. Pre-cleaned 7 mL Teflon beakers were placed under the columns and the sample solutions were loaded onto the resin. Two washes of 0.5 mL 7 M HNO<sub>3</sub> fully eluted the Ni while retaining Fe, Ti and V. After use, the columns were cleaned by filling with 18.2 M $\Omega$  cm water to remove any remaining Ni as well as Ti, V and Fe ready for reuse. The samples were dried down and treated overnight with one drop of 15.4 M HNO<sub>3</sub> at 160 °C.

### 2.3.4. Third column: AG50W-X8

It is important to remove from the samples any residual organic breakdown products resulting from the DMG and TruSpec resin. Again the columns used were 150  $\mu$ L and made of Teflon shrink fit. They were filled with pre-cleaned AG50W-X8 200–400 Biorad resin. Prior to each use the columns were cleaned with two passes of both 18.2 M $\Omega$  cm water and 6 M HCl. After cleaning, the columns were pre-conditioned with two aliquots of 0.5 mL of 0.25 M HCl. The samples were dried down, converted to chlorides with a single drop of 12 M HCl and dissolved in 1 mL of 0.25 M HCl. The samples were loaded and three aliquots of 0.5 mL of 0.25 M HCl were added to ensure that the sample and matrix was fully washed into the resin. Next, two aliquots of 2 mL of 0.25 M HCl were added to elute

fully any P present. Finally, clean beakers were placed under the column and the Ni was eluted with two aliquots of 0.5 mL of 4 M HCl. The samples were dried down, treated with one drop of 15.4 M HNO<sub>3</sub>, and dried down again.

### 2.3.5. Fourth column: AG-MP-1

This column removes any residual Zn or Zn contamination. It is of vital importance to ensure that the Zn in the analyte is reduced to as close to the level of the blank acid as possible, to minimise the magnitude of the required Zn correction, see Section 2.4.2. The columns used were again 150  $\mu$ L and made of Teflon shrink fit and were filled with Biorad AG-MP1. They were pre-cleaned with repeated rinsing with 6 M HCl and 18.2 M $\Omega$  cm water. Immediately prior to use, the columns were cleaned with two passes of 18.2 M $\Omega$  cm water and 0.3 M HNO<sub>3</sub> and a final pass of 18.2 M $\Omega$  cm water. The columns were then pre-conditioned with two aliquots of 0.5 mL of 1 M HCl. The samples were dissolved in 0.5 mL of 1 M HCl and loaded onto the columns. The Ni was collected with four aliquots of 0.2 mL of 1 M HCl. The samples were dried down with a single drop of 15.4 M HNO<sub>3</sub> and then dissolved in ~1 mL of 0.3 M HNO<sub>3</sub>. To avoid Zn contamination, the 0.3 M HNO<sub>3</sub> was added to the samples using a pre-cleaned wash bottle that was tested for Zn and Ni blanks prior to every use.

The Ni yield of the full analytical procedure was within error of 100%. Mass scans of cleaned matrix standards JP-1 (peridotite) and NIST SRM 361 (Ni-rich steel), show that there were trace levels of V, Cr and Mg. Separation factors, or the element/Ni ratio after chemistry divided by the element/Ni ratio before chemistry, for all elements are  $<2 \times 10^{-4}$ . However, accurate determinations of some separation factors were limited by low initial ratio, detection limit and reagent blanks. Elements with high initial ratios, in JP-1 for example Mg (initial Mg/Ni = 109, separation factor =  $2 \times 10^{-9}$ ), give a more realistic estimate of the extent of chemical separation. The elements that provide direct isobaric interferences, Fe and Zn, were also efficiently separated. Final Fe/Ni ratios are  $<3 \times 10^{-5}$  and Zn/Ni were in the range  $3 \times 10^{-7}$  to  $2 \times 10^{-5}$ . The typical Zn/Ni has decreased during the study as improved handling methods have reduced Zn contamination. The effects of Fe and Zn interferences on the accuracy of Ni isotope measurements are discussed in Section 2.4.2. The total procedural blank of the chemistry was  $<20$  ng both for samples initially processed by Regelous et al. (2008), and during this study. These blanks are negligible compared to the ~50–1000  $\mu$ g of Ni normally processed through the chemistry. Blanks and separation factors were determined on a Thermo Finnigan Element 2, calibrated with standards diluted from a 1000 ppm CPI Ni concentration standard.

### 2.3.6. Chemical purification of sulphides

For sulphides a slightly different chemical separation procedure was required, because after complete dissolution in HCl the sulphide PtYG (see Section 2.1) was found to be insoluble in HNO<sub>3</sub>. This procedure uses the same columns in a slightly different order.

To remove the major Fe component, the PtYG was passed through a larger version of column four

(Section 2.3.5) with a 1 mL resin bed. The loading and elution volumes were scaled up directly and the calibration of the Ni elution found to be identical. After this column the samples were dried down and taken up in 0.25 M HCl and passed through the third column from the main chemistry, exactly as described above, Section 2.3.4. This column removed the matrix component that was insoluble in HNO<sub>3</sub>. To finish the chemical purification of sulphides, samples were passed through the first column as described above (Section 2.3.2) in order to separate any remain matrix elements. Then samples were treated to breakdown DMG and passed through the final cleanup column (column four, Section 2.3.5) to reduce Zn and Fe to background levels for analysis.

## 2.4. Mass spectrometry

### 2.4.1. Sample introduction, cup configuration and gas interferences

The isotope ratios of Ni solutions were determined using a Thermo-Finnigan Neptune multiple-collector inductively-coupled plasma mass spectrometer (MC-ICP-MS) (Bristol Neptune 1, Serial No. 1002), in medium resolution mode (with  $M/\Delta M \geq 6000$ , see below). Solutions of Ni separated from samples and dissolved in 0.3 M HNO<sub>3</sub> were introduced into the mass spectrometer, via a  $<50 \mu\text{L min}^{-1}$  nebuliser and a Cetac Aridus desolvator. The spray chamber was heated to 105 °C and the desolvating membrane was heated to 160 °C. The Ar sweep gas, optimised for signal intensity, was in the range 5–7 L min<sup>-1</sup>. Nitrogen was bled into the post desolvation sample stream and optimised for lowest Zn/Ni and ranged from 2 to 5 mL min<sup>-1</sup>, see Section 2.4.2. The Faraday cups collecting <sup>58</sup>Ni and <sup>60</sup>Ni were connected to amplifiers with  $10^{10} \Omega$  feedback resistors, while all other cups were connected to amplifiers with  $10^{11} \Omega$  feedback resistors. This feedback resistor configuration allows a maximum <sup>58</sup>Ni beam current of 5000 pA to be measured. Sample solutions were diluted with 0.3 M HNO<sub>3</sub> to give  $\sim 3500$  pA of <sup>58</sup>Ni. If the amount of sample available was limited, solutions were simply made up to the 4 mL required for the analysis. All sample intensities, including those at reduced intensity, were matched to the intensity of bracketing standards to within 5%. All amplifiers ( $10^{10} \Omega$  and  $10^{11} \Omega$ ) were calibrated using a highly stable current of nominally 333 pA, integrating for 30 s. In addition any artefacts produced by nonlinearity of the amplifiers is removed by a second normalisation, achieved by sample standard bracketing, see Section 2.4.3. Nickel sample and skimmer cones were used for this study because it was found they gave lower, more stable, instrumental Ni blank,  $<0.1$  pA, than Pt tipped cones.

The cup configuration permits measurement of all Ni isotopes and <sup>66</sup>Zn to be made simultaneously (see Table 1) allowing for the correction of the interference of <sup>64</sup>Zn on <sup>64</sup>Ni. However, in order to correct for the <sup>58</sup>Fe interference on <sup>58</sup>Ni, another Fe isotope must be collected. Unfortunately, the dispersion of the Neptune is not great enough to cover the range 57–66 AMU, without using the zoom quadrupole lenses, which has a detrimental effect on the peak shape. Since measurements are made in medium reso-

lution, close to the peak edge, we could not accept any compromise in peak shape. Therefore, in order to correct for the <sup>58</sup>Fe interference on <sup>58</sup>Ni, the <sup>56</sup>Fe/<sup>62</sup>Ni ratios were determined in a separate measurement with the magnet set to a lower mass, Table 1. For both the Ni and Fe measurement configurations, an average ‘on-peak’ blank, from measurements bracketing each sample or standard, was subtracted from the mean of that sample or standard analysis. The blank solution measured was the same solution used to dissolve and dilute the samples.

A typical analytical session consisted of three samples, each measured four times for 100 cycles of 8.39 s integration time, with each sample measurement bracketed by a standard measurement also of 100 cycles of 8.39 s. All of these measurements were interleaved with 25 cycles of 8.39 s comprising the on-peak blank measurement. After these were complete, the Fe/Ni ratios of all samples and standards were measured after a magnet jump to collect <sup>56</sup>Fe in L3 (Table 1) with 25 cycles of 8.39 s. These Fe/Ni ratios measurements were also blank corrected. A peak centre was performed during every measurement of a sample or a standard.

As described above (Section 1), the Ni mass spectrum suffers from molecular interferences generated from the plasma gas. It was suggested by Chen et al. (2009) that such molecular interferences (though they did not specify which) present a serious analytical concern. However, we analysed the samples using a mass resolution of  $M/\Delta M \geq 6000$ , where  $\Delta M$  is the peak edge width measured from 5% to 95% of peak height, which resolves the plasma gas interferences from the Ni beams. For example, <sup>40</sup>Ar<sup>18</sup>O mass = 57.9615 AMU can be resolved from <sup>58</sup>Ni (mass = 57.9353 AMU) with a nominal resolution of  $M/\Delta M = 2250$ . Due to the use of different medium resolution slits, focus settings and measurement positions over the course of the study, the degree to which molecular species were resolved changed. The poorest resolved species (except for hydrides) is <sup>40</sup>Ar<sup>18</sup>O, which was resolved in the worst case at 2% of its peak intensity but typically much better. In this worst case, using the highest observed <sup>40</sup>Ar<sup>18</sup>O, this corresponds to an unresolved component added to the <sup>58</sup>Ni beam of 2 ppm which is, in any case, corrected for by the on-peak blank subtraction. The sample standard bracketing, or second normalisation see Section 2.4.3, will also remove any contribution from scattered ions, assuming the scattered ion/Ni ratio is the same for samples and standards.

The proximity of the measurement (axial) mass setting to both the peak edge and the interferences was assessed by making isotope ratio measurements over a range of axial masses using a technique similar to that described by Weyer et al. (2003). This procedure was routinely carried out after setting the cup positions before collecting any data. For the geometry of the Neptune a difference of one mAMU in the mass range corresponds to a difference of 18  $\mu\text{m}$  in cup position. The cups were set to a reproducibility of  $\pm 10 \mu\text{m}$  total range. At each axial mass setting the measurement was corrected for interferences on <sup>64</sup>Ni (see Section 4.3) and internally-normalised to <sup>58</sup>Ni/<sup>61</sup>Ni to correct for mass bias. A second normalisation was applied by calculating the epsilon unit variation from the isotope ratio corresponding to

Table 1

The cup configuration and principal ion beams collected in both the main and Fe correction magnet position. Also shown is a non-exhaustive list of example isobaric interferences. Elemental interferences are reduced by chemical separation and corrected by peak stripping. Gas interferences are mass resolved under the medium resolution measurement conditions.

	Cup									
	L4	L3	L2	L1	C	H1	H2	H3	H4	
Isotope	<sup>58</sup> Ni	—	<sup>60</sup> Ni	<sup>61</sup> Ni	<sup>62</sup> Ni	—	<sup>64</sup> Ni	—	<sup>66</sup> Zn	
Elemental isobar	<sup>58</sup> Fe	—	—	—	—	—	<sup>64</sup> Zn	—	—	
Gas interference	<sup>40</sup> Ar <sup>18</sup> O	—	<sup>40</sup> Ar <sup>20</sup> Ne	<sup>40</sup> Ar <sup>21</sup> Ne	<sup>40</sup> Ar <sup>22</sup> Ne	—	<sup>32</sup> S <sup>16</sup> O <sub>2</sub>	—	<sup>40</sup> Ar <sup>12</sup> C <sup>14</sup> N	
Fe jump	—	<sup>56</sup> Fe	—	—	—	—	—	<sup>62</sup> Ni	—	
Gas interference	—	<sup>40</sup> Ar <sup>16</sup> O	—	—	—	—	—	<sup>40</sup> Ar <sup>22</sup> Ne	—	

the axial mass employed for data collection (61.899 AMU). This normalisation procedure allows us to average data from a representative selection of 21 analytical sessions to obtain high precision determinations and these averages are plotted in Fig. 1(a)–(c).

Fig. 1(d) shows the variation in the peak centre during a typical analytical session, that is the corrections made by the peak centering routine at the beginning of each analysis. At the beginning of each sample or standard a peak centre was performed to exactly align the centre cup to the reference position (the zero point in Fig. 1(d)). The 2 standard deviations (2 SD) variation of the peak centre correction is <1 mAMU and the largest deviation is ~1 mAMU. With this magnitude of variation the measurement position is stable and resolved from both the peak edge at -2 mAMU and the onset of the interferences at +7 mAMU, see Fig. 1(b). The contribution of <sup>40</sup>Ar<sup>12</sup>C<sup>14</sup>N to <sup>66</sup>Zn, causing an overcorrection for <sup>64</sup>Zn to <sup>64</sup>Ni is evident 9 mAMU beyond the reference mass in Fig. 1(c).

The location of the measurement position was chosen to be as close as possible to the peak edge to ensure resolution of any (scattered) interferences, while being stable enough to not slip off the peak edge. As the study progressed, additional data allowed us to define the topography of the peak edge more precisely and lead us to move the measurement position to slightly higher mass (+2 mAMU). This change makes the measurement more robust to anomalously large magnet drifts, but does not otherwise affect the results. Our measurement position is on the hydride influenced portion of the peak because the uninterfered Ni peaks are not fully resolved. This minor hydride contribution should be removed by sample-standard bracketing, since the samples and standards should be equally affected. When measured the hydride formation is less than 1 ppm of the Ni beam. Fig. 1 shows that, within the precision of the measurements, ~0.1‰ 2 standard errors (2 SE), there is a mass range of ~10 mAMU in which all beams have fully entered the cups but there are no contributions from interferences, except hydrides.

#### 2.4.2. Elemental interference corrections, Fe/Ni and Zn/Ni

Nickel also suffers elemental isobaric interferences, <sup>58</sup>Fe on <sup>58</sup>Ni and <sup>64</sup>Zn on <sup>64</sup>Ni, which are tackled in two ways: effective chemical separation (see Section 2.3) and correction of the raw data by peak stripping.

Correction for the interference of <sup>58</sup>Fe on <sup>58</sup>Ni is achieved by measuring the <sup>56</sup>Fe/<sup>62</sup>Ni in a post main-run

sub-routine after changing the axial mass setting (see Section 2.4.1). The interfering <sup>58</sup>Fe intensity is calculated for each measurement of sample or standard, from the 'reference' <sup>58</sup>Fe/<sup>56</sup>Fe [0.00307,] (Taylor et al., 1992), and is subtracted from the <sup>58</sup>Ni intensity, prior to the mass bias correction. Due to the use of <sup>58</sup>Ni, along with <sup>61</sup>Ni, as a normalising isotope, any error in its measurement, for example from an inaccurate Fe correction, will propagate into all the normalised data. Thus, although the Fe correction is straightforward to achieve, it is important to assess the effects of its application. The highest measured <sup>56</sup>Fe intensity is 1 pA and the average is 0.03 pA. This means the highest contribution of <sup>58</sup>Fe to <sup>58</sup>Ni is 0.003 pA and the average is 0.0001 pA. When compared to the <sup>58</sup>Ni beam which is always >700 pA and typically ~3500 pA, it is clear that this is a negligible contribution. In the worst case it is a 5 ppm correction to the <sup>58</sup>Ni beam. One differently processed sample, Skookum, which was kindly provided by Martin Bizzarro contained significantly more Fe, Fe/Ni ratio =  $4.6 \times 10^{-3}$  which is somewhat higher than the level of Fe contamination reported by Bizzarro et al. (2007), Fe/Ni ratio ~ $1.2 \times 10^{-3}$ . This discrepancy may result from the different instruments used, with different ionisation efficiencies of Fe relative to Ni, or because of the extra transport and handling this sample underwent. Even though this sample had more than an order of magnitude more Fe than our other analyses of IVB iron meteorites, the isotope ratios measured are identical, within error, to the average of the other IVBs, see Table 2 (with the exception of Tlacotepec which is thought to have been perturbed by spallation, see Section 4.5).

The separation of Zn from Ni is difficult to maintain because Zn is a ubiquitous contaminant in reagents and the environment. In addition, <sup>64</sup>Zn is the most abundant Zn isotope (48.6% of total Zn) and <sup>64</sup>Ni is the least abundant Ni isotope (only 0.93% of total Ni). Therefore, an accurate Zn correction is more difficult to achieve. After chemical separation and dilution, see Section 2.3.5, the Zn concentration approaches the level of the blank acid. In order to reduce the influence of this residual Zn during the measurement, N<sub>2</sub> gas was routinely bled into the post desolvation sample line. The addition of N<sub>2</sub> has the effect of reducing both Zn/Ni and Ni intensity. Thus, it is important to balance the reduced Zn/Ni with the loss of Ni signal. After altering the N<sub>2</sub> flow rate the Ar sweep gas was again optimised for maximum intensity. Typically the optimum N<sub>2</sub> flow rate for lowest Zn/Ni resulted in a loss of 10–15% of

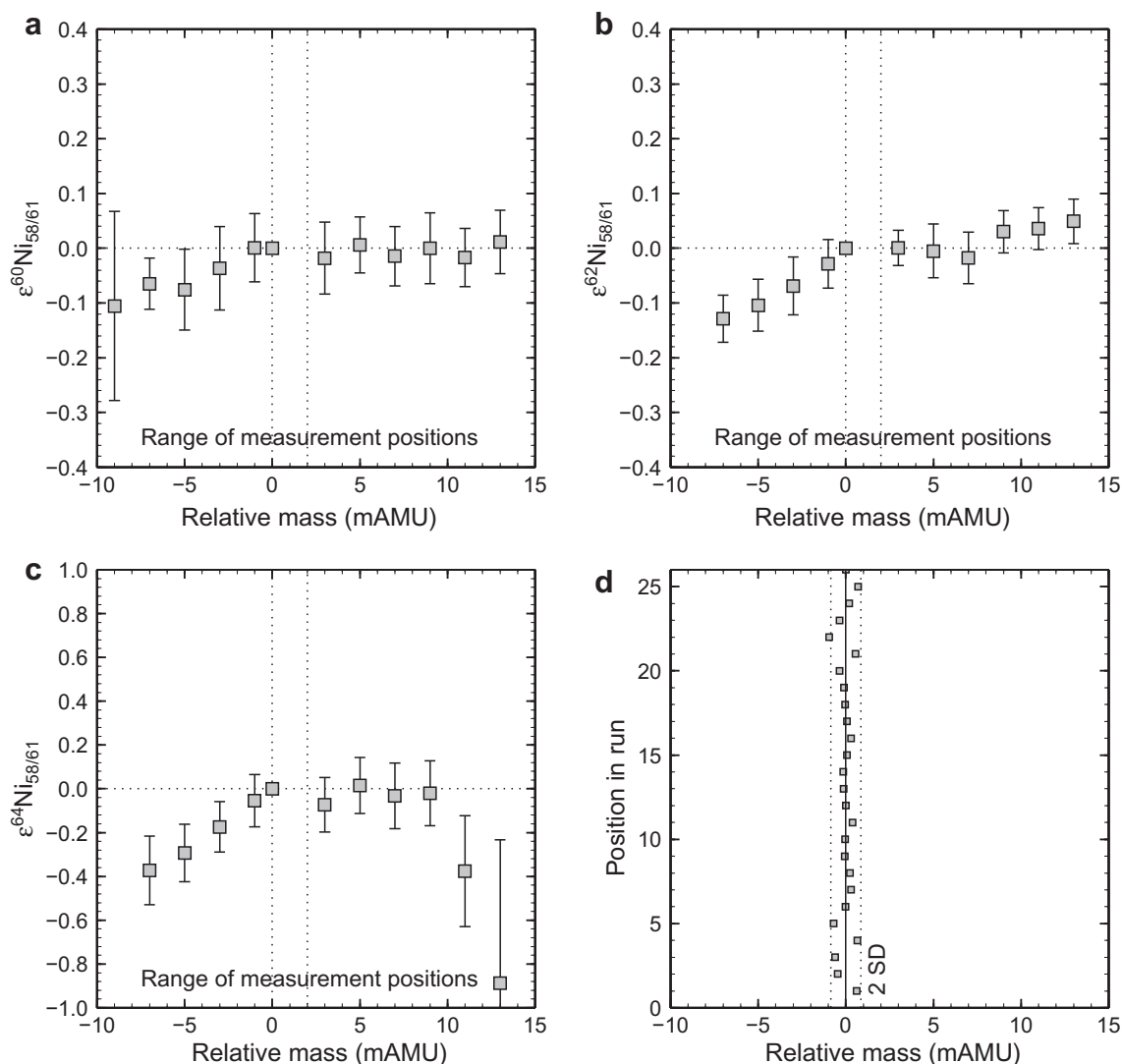


Fig. 1. (a–c) Plots showing the variation of the internally normalised isotope ratio across the peak flat to illustrate the proximity of the peak edge and the gas interferences. *x*-axis – distance from measurement position in mAMU. Plots show there is a flat of at least 11 mAMU. (d) Plot shows the variation of the peak centre during all the Ni analyses of a single analytical session.

the Ni signal. This loss in Ni intensity was accompanied by a drop of a factor of two in Zn/Ni. Although not used in every analytical session,  $\text{N}_2$  was used in the majority. There is no difference outside error between samples or standards analysed with or without  $\text{N}_2$ . A potential inaccuracy of a Zn interference correction is mass fractionation of Zn isotopes in the mass spectrometer. To address this problem we use the Ni mass bias factor ' $\beta$ ' of the exponential law (Russell et al., 1978) to calculate an instrumentally fractionated  $^{64}\text{Zn}/^{66}\text{Zn}$ , from the reference  $^{64}\text{Zn}/^{66}\text{Zn}$ . This was calculated for each individual measurement in a sequence. The calculated  $^{64}\text{Zn}$  intensity is then subtracted from the mass-64 intensity for each measurement of the sample or standard. The Zn correction of the  $^{64}\text{Ni}$  ranged from 13 to 520 ppm.

The effectiveness of our Zn correction for different measured Zn/Ni ratios is shown in Fig. 2, which comprises separate averages of four repeat measurements from individual

analytical sessions. The  $\epsilon^{64}\text{Ni}_{58/61}$  of terrestrial samples are offset from zero due to expected fractionation effects, see Section 4.1. The data in Fig. 2 have been processed to remove this offset, see the caption of Fig. 2 for details. In order to ensure there was no discernible contribution to  $\epsilon^{64}\text{Ni}_{58/61}$  from  $^{64}\text{Zn}$ , we placed a conservative upper limit on Zn/Ni for acceptable analyses at  $1.5 \times 10^{-5}$ . This limit corresponds to a maximum possible correction of  $\sim 600$  ppm. The inset of Fig. 2 shows an expanded view of data below the 'cut off'.

#### 2.4.3. Mass bias corrections

Instrumental and natural mass fractionation were corrected by internal normalisation to  $^{58}\text{Ni}/^{61}\text{Ni} = 59.722$  (Gramlich et al., 1989a,b) using the exponential law (Russell et al., 1978). Two different normalising ratios,  $^{58}\text{Ni}/^{61}\text{Ni}$  and  $^{58}\text{Ni}/^{62}\text{Ni}$ , have been used in previous studies of mass-independent Ni isotope variations. We favour

Table 2

Ni isotopic data obtained during this study. All data are reported relative to the NIST SRM 986 Ni isotopic standard (Gramlich et al., 1989a). Some  $\delta^{60/58}\text{Ni}$  obtained by Cameron et al. (2009) marked by \*, some original to this study. All meteorite samples, except Skookum, were dissolved and initially processed by Regelous et al. (2008); before analysis these solutions were passed through anionic exchange resin (see Section 2.3.5) in order to remove residual Zn. NIST SRM361 and JP-1 have been processed both by Regelous et al. (2008) and during this study. NIST SRM 986-col has been processed through the full chemical separation procedure. The  $\epsilon^{60}\text{Ni}_{61}$  and  $\epsilon^{62}\text{Ni}_{61}$  data presented here is identical within error to that of Regelous et al. (2008), though at slightly higher precision. CoGH stands for Cape of Good Hope. The best estimate of the Bulk Silicate Earth shown is the weighted mean of the two peridotite samples, JP-1 and DTS-2.

Sample	Group	NHM No.	<i>n</i>	<i>n</i> <sub>64</sub>	$\epsilon^{60}\text{Ni}_{61}$	2 SE	$\epsilon^{62}\text{Ni}_{61}$	2 SE	$\epsilon^{64}\text{Ni}_{61}$	2 SE	$\delta^{60/58}\text{Ni}$	2 SE
<i>Iron meteorites</i>												
Tlacotepec	IVB	1959,913	4	4	-0.136	0.019	0.023	0.015	0.134	0.058	—	—
Santa Clara	IVB	1983,M27	16	4	-0.121	0.017	0.087	0.040	0.369	0.073	0.320	0.027
Hoba	IVB	1930,976	8	8	-0.122	0.017	0.084	0.016	0.214	0.049	0.330*	0.060
CoGH	IVB	1985,M246	4	4	-0.126	0.005	0.099	0.006	0.271	0.056	—	—
Skookum	IVB	—	4	4	-0.129	0.038	0.067	0.048	0.168	0.073	—	—
Putnam County	IVA	90,228	8	8	-0.049	0.019	-0.069	0.033	-0.243	0.079	—	—
Bristol	IVA	1955,226	16	8	-0.048	0.020	-0.047	0.026	-0.165	0.057	0.280*	0.050
Bendegó	IC	66,585	4	4	-0.013	0.019	-0.001	0.027	-0.030	0.075	—	—
Arispe	IC	86,425	4	4	-0.049	0.026	-0.129	0.049	-0.317	0.092	—	—
Lenarto	IIIAB	61,304	4	4	-0.047	0.029	-0.083	0.036	-0.318	0.113	—	—
Henbury	IIIAB	—	4	4	-0.056	0.024	-0.090	0.044	-0.304	0.045	0.240*	0.070
Coahuila	IIAB	54,242	4	4	-0.031	0.017	-0.088	0.040	-0.259	0.034	0.360*	0.040
<i>Terrestrial standards</i>												
NIST SRM 361	T	—	72	41	-0.011	0.007	0.029	0.013	0.136	0.033	-0.039	0.032
NIST SRM 986-col	T	—	4	4	0.002	0.006	-0.024	0.028	0.000	0.042	—	—
CPI	T	—	16	12	0.002	0.010	0.017	0.016	0.083	0.031	0.101	0.024
NiSalt	T	—	16	16	-0.016	0.009	0.058	0.018	0.226	0.048	0.470*	0.080
PtYG	T	—	20	20	0.010	0.008	-0.009	0.017	0.012	0.033	-0.645	0.080
JP-1	T	—	58	50	-0.006	0.007	0.035	0.010	0.117	0.021	0.100	0.080
DTS-2	T	—	4	4	-0.007	0.032	0.038	0.063	0.161	0.100	0.128	0.080
Bulk Silicate Earth	T	—	—	—	-0.006	0.007	0.036	0.010	0.119	0.021	0.179	0.036

normalisation to  $^{58}\text{Ni}/^{61}\text{Ni}$  because previous studies have reported anomalies in both  $\epsilon^{62}\text{Ni}_{61}$  and  $\epsilon^{64}\text{Ni}_{61}$  for CAIs (Birck and Lugmair, 1988) and  $\epsilon^{62}\text{Ni}_{61}$  in bulk samples (Regelous et al., 2008) that are in keeping with nucleosynthetic theory (e.g. Woosley, 1997).

Internal normalisation should correct for both instrumental and natural mass-dependent fractionation, however, several studies have highlighted that at high precision a small residual effect may remain in the normalised data (Vance and Thirlwall, 2002; Wombacher et al., 2004). These studies find empirical solutions to these problems: either by applying a post-normalisation correction to a second isotope pair (Vance and Thirlwall, 2002); or the use of the generalised power law (GPL) (Maréchal et al., 1999) in the case of Wombacher and Rehkämper (2003). The first option is not open to us because we are investigating mass-independent isotopic variability in stable isotope ratios in addition to radiogenic isotope ratios. Nickel only has five isotopes, so four independent ratios, three of which are expected to have anomalies and cannot be assumed to be constant. Secondly, as noted by Wombacher and Rehkämper (2003), the use of the GPL with an empirically optimised ‘*n*-value’ is not a realistic option for routine isotope work at this time. Thus a second normalisation was applied by calculating the relative deviation of samples from a linear regression through bracketing measurements of NIST SRM 986 (as in Regelous et al., 2008); this is commonly referred to as

sample-standard bracketing. Wombacher and Rehkämper (2003) also noted that applying such a second normalisation is a valid solution to the problem of non-exponential instrumental mass-fractionation. Data are reported using the  $\epsilon$  notation (‰) relative to these bracketing standards, see Eq. (1). A full assessment of the possible contribution of mass-dependent fractionation to mass-independent data is given in Section 4.1.

#### 2.4.4. Determination of mass-dependent fractionation by double-spike

The mass-dependent Ni isotope fractionation relative to NIST SRM 986 of some samples and standards were determined by a Ni double-spike technique described by Cameron et al. (2009), who also previously reported data for a number of samples used in this study from the same dissolutions, (see Table 2). The isotopes used in the double-spike are  $^{61}\text{Ni}$  and  $^{62}\text{Ni}$ , obtained from Oak Ridge National Laboratories, mixed in roughly equal proportions. The precise isotopic composition of the spike was calibrated as described in Cameron et al. (2009) and references therein. The ratios used for the double-spike inversion were,  $^{60}\text{Ni}/^{58}\text{Ni}$ ,  $^{61}\text{Ni}/^{58}\text{Ni}$  and  $^{62}\text{Ni}/^{58}\text{Ni}$ . The samples were analysed on the second Thermo-Finnigan Neptune MC-ICP-MS (Serial No. 1020) in Bristol. Meteorite samples from Cameron et al. (2009) were spiked prior to chemistry, while samples analysed for mass-dependent fractionation during

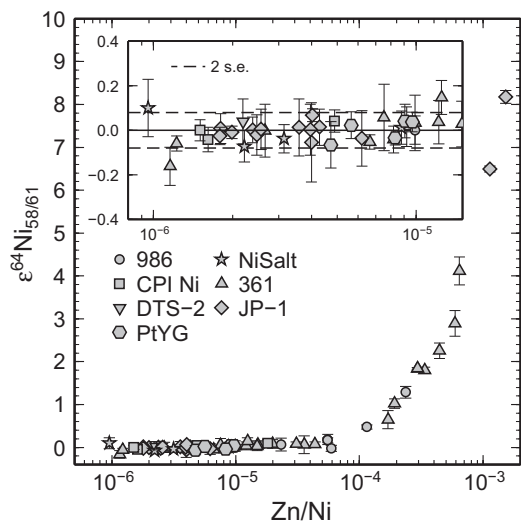


Fig. 2. Plot showing the effect of increasing Zn/Ni on fully processed  $\epsilon^{64}\text{Ni}_{58/61}$ . The plot shows that an accurate Zn correction is vital for accurate  $\epsilon^{64}\text{Ni}_{58/61}$  and that the cut-off for acceptable  $\epsilon^{64}\text{Ni}_{58/61}$  is a Zn/Ni in the  $10^{-5}$  range. The samples with Zn/Ni ratios higher than  $10^{-4}$  were spiked with Zn using an aliquot diluted from a 1000 ppm CPI ICP-MS Zn concentration standard. Each datum comprises four repeat measurements of a standard collected during a single analytical session. As discussed in Section 4.1, terrestrial samples are offset from zero due to expected fractionation effects. To remove this offset, deviations from the mean of the low Zn measurements ( $\text{Zn/Ni} < 1.5 \times 10^{-5}$ , see text) have been calculated individually for each sample. The inset figure displays an expanded view of the 'cut off' region.

this study were spiked after chemical separation. Thus, the approach of Cameron et al. (2009) corrects for any fractionation that occurred during chemical separation, while the fractionation measured on samples in this study includes fractionation, if any, that occurred on the columns. Duplicate samples, e.g. CI Orgueil, which were determined on aliquots both spiked before and after chemistry yield mass-dependent results within error of each other ( $\delta^{60/58}\text{Ni} = 0.21 \pm 0.07\text{‰}$ , Cameron et al. (2009) and  $\delta^{60/58}\text{Ni} = 0.18 \pm 0.02\text{‰}$ , this study). This shows that significant fractionation does not occur during chemical separation.

### 3. RESULTS

#### 3.1. Mass-independent data

Mass-independent Ni isotope data obtained for a range of terrestrial standards and 12 iron meteorite samples are reported in Table 2 and plotted in Fig. 3. The data show a range of  $0.146\text{‰}$ ,  $0.228\text{‰}$  and  $0.687\text{‰}$  for  $\epsilon^{60}\text{Ni}_{58/61}$ ,  $\epsilon^{62}\text{Ni}_{58/61}$  and  $\epsilon^{64}\text{Ni}_{58/61}$ , respectively. There is a strong positive correlation between  $\epsilon^{62}\text{Ni}_{58/61}$  and  $\epsilon^{64}\text{Ni}_{58/61}$  in iron meteorites with a slope of  $3.03 \pm 0.71$ , determined by York regression (York, 1968). Conversely, between  $\epsilon^{60}\text{Ni}_{58/61}$  and  $\epsilon^{62}\text{Ni}_{58/61}$  there is no overall correlation. Notably, the terrestrial standards do not all yield  $\epsilon^{60}\text{Ni}_{58/61}$ ,  $\epsilon^{62}\text{Ni}_{58/61}$  or  $\epsilon^{64}\text{Ni}_{58/61}$  values within error of zero as defined by the NIST SRM 986 (for reasons discussed in Section 4.1), but this variability is substantially

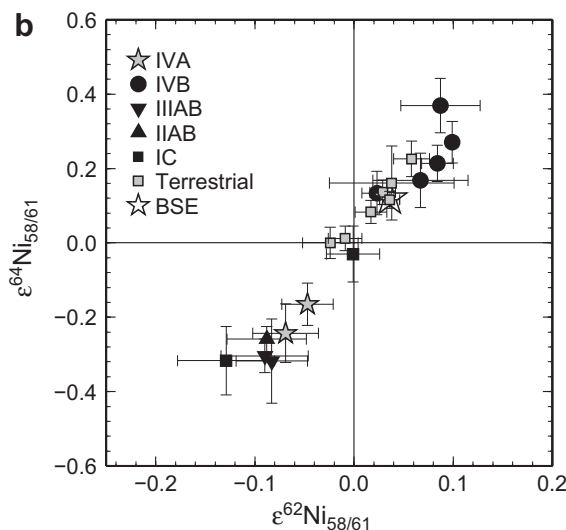
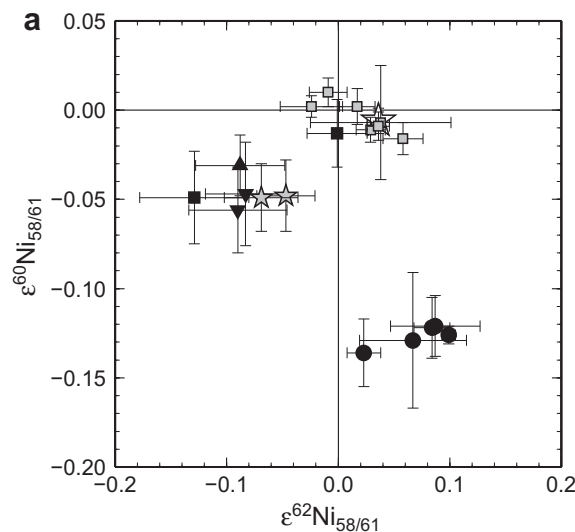


Fig. 3. Plots showing mass-independent Ni isotopic data collected during this study for five iron meteorite groups and terrestrial standards. The terrestrial standards show an array consistent with fractionation during different processes, see Section 4.1.

less than that displayed by the iron meteorites. Of the iron meteorite samples none show isotopic compositions within error of natural terrestrial materials (see Section 4.1).

#### 3.2. Mass-dependent data

Double-spiked, mass-dependent Ni isotope variations in iron meteorite samples from this study and Cameron et al. (2009) are reported in Table 2 and plotted in Fig. 4. These data show a range in  $\delta^{60/58}\text{Ni}$  of  $0.24\text{--}0.36\text{‰}$ . By definition NIST SRM 986 is zero. The iron meteorites show a near constant offset relative to this reference ( $\delta^{60/58}\text{Ni} \sim 0.3\text{‰}$ ) but other terrestrial samples are variably fractionated, ranging from PtYG with  $\delta^{60/58}\text{Ni} = -0.65\text{‰}$  to the NiSalt with  $\delta^{60/58}\text{Ni} = 0.47$ . Taken as a whole the meteorite and terrestrial data show no correlation between mass-dependent and mass-independent ratios (Fig. 4); terrestrial ratios

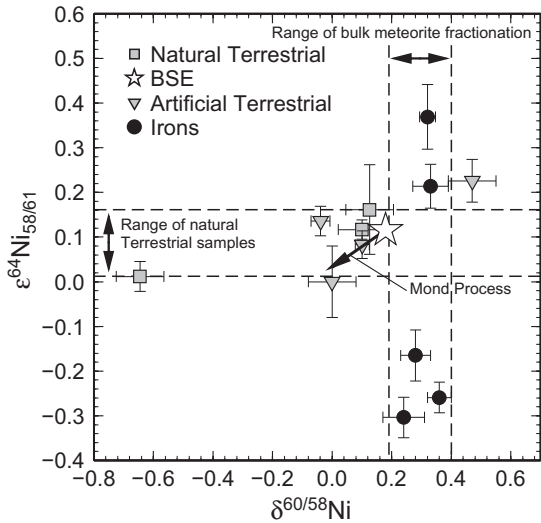


Fig. 4. Plot of mass-dependent  $\delta^{60/58}\text{Ni}$  vs. mass-independent  $\epsilon^{64}\text{Ni}_{58/61}$ . All data reported were measured on the same dissolutions. Some of the  $\delta^{60/58}\text{Ni}$  data are from Cameron et al., 2009 and some are original to this study. The lack of correlation is strong evidence that, within the levels of precision, the mass-independent variability is not a consequence of inaccurate correction of mass fractionation.

dominate the variation in mass-dependent fractionation, whereas mass-independent variations are principally evident in meteorites. Mass-dependent data for bulk iron meteorites and sulphides were previously reported by Cook et al. (2006). The bulk data reported by Cook et al. (2006) are consistent, within error, with the data reported in this study.

#### 4. DISCUSSION

Before interpreting  $0.1\text{‰}$  variations in Ni isotope ratios of samples (Fig. 3), a clear demonstration is required of the reliability of the measurements to such high levels of precision. The following is a detailed discussion of analytical issues that surround the measurement and reporting of high precision isotopic anomalies. The majority of these issues are widely applicable to many isotopic system, but some are specific to Ni.

##### 4.1. Accuracy

In order to assess the accuracy of our meteorite data we have measured seven terrestrial materials. Note that by ‘accuracy’ we mean that relative to the NIST SRM 986 Ni isotopic standard and do not make any claims to accuracy of the absolute ratios since NIST SRM 986 is certified only to  $\sim 3\text{‰}$  ( $\sim 7\text{‰}$  for  $^{64}\text{Ni}/^{60}\text{Ni}$ ). As described above these comprise four artificially processed standards: NIST SRM 986, NIST SRM 361, CPI and NiSalt; and three natural materials: JP-1, DTS-2 and PtYG. Figs. 3 and 5 show that terrestrial materials are negatively correlated in  $\epsilon^{62}\text{Ni}_{58/61}$  vs.  $\epsilon^{60}\text{Ni}_{58/61}$  and positively correlated in  $\epsilon^{62}\text{Ni}_{58/61}$  vs.  $\epsilon^{64}\text{Ni}_{58/61}$ . One end of the array is defined by NIST SRM 986 and PtYG and the other by NiSalt. We note that the samples PtYG and NiSalt also form the extremes of the mass-dependent range

(Fig. 4) and that NIST SRM 986 and NiSalt are highly purified artificial standards. By comparison with the meteorite variability the range in  $\epsilon^{60}\text{Ni}_{58/61}$ ,  $\epsilon^{62}\text{Ni}_{58/61}$  and  $\epsilon^{64}\text{Ni}_{58/61}$  of the natural terrestrial materials is small,  $0.019\text{‰}$ ,  $0.047\text{‰}$  and  $0.104\text{‰}$ , respectively, between PtYG and BSE (see below). This range is similar to the typical external precision of four repeat measurements and within the precision of all previous Ni isotope studies.

In this study,  $\epsilon = 0$  is defined by analyses of aliquots of NIST SRM 986 solution which have not been passed through the Ni purification procedure. The sample ‘NIST SRM 986-col’ is the same solution that has passed through chemistry and yields results within error of zero. This suggests that there is no bias introduced by the chemical separation procedure itself. In addition, multiple dissolutions of the two peridotites, JP-1 and DTS-2, and the metal

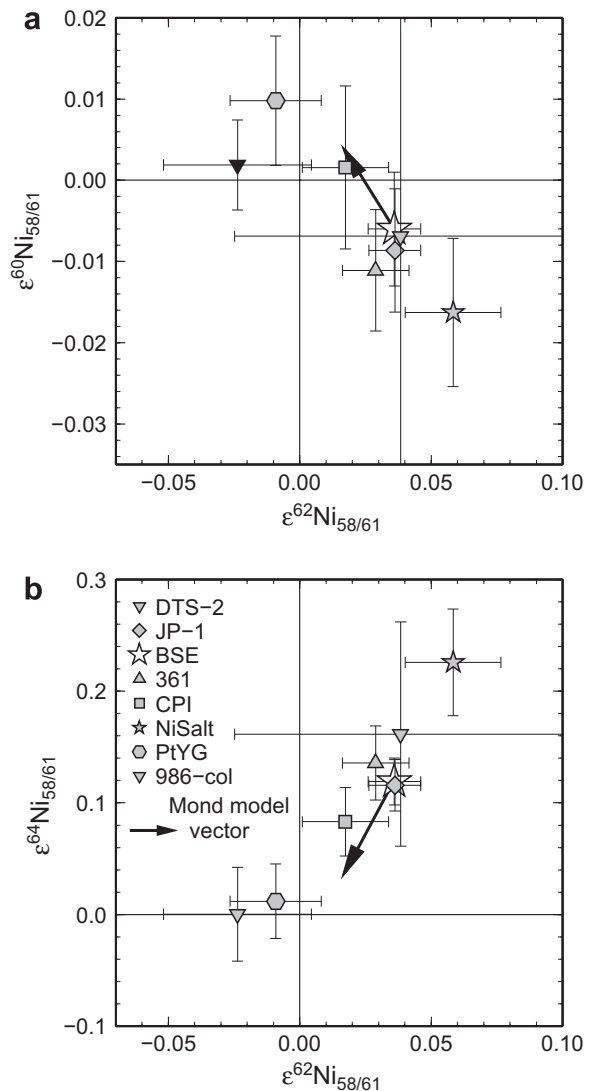


Fig. 5. Plots showing that the composition of NIST SRM 986 may be consistent with mass-dependent fractionation occurring as  $\text{Ni}(\text{CO})_4$  during the Mond process, where the starting composition is identical to BSE. See main text for more detail.

standard NIST SRM 361, which have very different matrices, yield identical results within error. All this evidence strongly suggests that the range of ratios in the terrestrial samples is not the product of some residual matrix, interference or column fractionation. This leads us to question whether the expectation that all terrestrial samples must yield identical mass-independent ratios is reasonable.

In order to correct for the effects of natural mass-dependent processes a ‘law’ describing the style of fractionation must be assumed. Theoretical descriptions of end-member processes, e.g. equilibrium (Bigeleisen and Mayer, 1947) or kinetic (Bigeleisen, 1949), show divergent behaviour which is most marked for highly fractionated systems. Thus, if natural samples were highly mass-fractionated by a different law or as different species to that used to correct for instrumental mass bias (kinetic elemental fractionation) residual, apparent mass-independent anomalies will result, see Young et al. (2002) for a full discussion. Young et al. (2002) noted that the assumption of a single mass-dependent law to correct for all natural and instrumental fractionation is not valid and that the inaccuracies inherent in making such a simplification will become increasingly apparent as analytical precision improves due to technical and instrumental advances. Therefore, small differences in mass-independent ratios from a variety of terrestrial materials may be unavoidable.

If natural mass-dependent fractionation is inadequately corrected, the most fractionated samples should have the most extreme mass-independent isotopic ratios. Indeed, mass-dependent isotope ratios in the terrestrial materials are broadly correlated with their mass-independent ratios (Fig. 4) as might be anticipated from the discussion above. Moreover, Fig. 4 there is no correlation in the meteorite samples between  $\epsilon^{64}\text{Ni}_{61}^{38}$  and  $\delta^{60/58}\text{Ni}$ . The full range in  $\epsilon^{64}\text{Ni}_{61}^{38}$  occurs in iron meteorites with indistinguishable  $\delta^{60/58}\text{Ni}$ . Moreover, terrestrial samples cover approaching an order of magnitude larger range in  $\delta^{60/58}\text{Ni}$  of the meteorites and show only a subtle difference in mass-independent ratios (as discussed above). Thus, imperfect correction of natural mass-dependent fractionation cannot account for the variability of mass-independent Ni isotope ratios seen in the iron meteorites.

The mantle is the major repository of Ni in the silicate Earth and therefore the peridotites probably best represent the isotopic composition of the BSE. For the purposes of this study we define the mass-independent ratios of the BSE as the averages of all 54 measurements of JP-1 and 4 measurements of DTS-2, these are  $\epsilon^{60}\text{Ni}_{61}^{38} = -0.006 \pm 0.007\text{‰}$ ,  $\epsilon^{62}\text{Ni}_{61}^{38} = 0.036 \pm 0.010\text{‰}$  and  $\epsilon^{64}\text{Ni}_{61}^{38} = 0.119 \pm 0.021\text{‰}$ . The mass-dependent composition of the BSE is defined as the average of high Ni, mantle derived samples from Cameron et al. (2009) and this study:  $\delta^{60/58}\text{Ni} = 0.179 \pm 0.036\text{‰}$ .

As an example of how the convention of correcting all mass-dependent fractionation, both instrumental and inherent within the sample, using atomic masses and the exponential (kinetic) law can lead to mass-independent anomalies we explore the production purified Ni by the Mond process (Mond et al., 1890; Roberts-Austen and November, 1898). This may have some relevance for mass-independent variability of the Ni standards. The

Mond process uses the extreme volatility, and thermal instability of nickel tetracarbonyl ( $\text{Ni}(\text{CO})_4$ ) to purify Ni. Carbon monoxide is passed over Ni powder at 50 °C forming  $\text{Ni}(\text{CO})_4$  gas, which is then removed to a different chamber and undergoes decarbonylation reaction by contact with high temperature ( $\sim 200$  °C) Ni nucleation sites. During the Mond process Ni may thus experience mass fractionation as the species  $\text{Ni}(\text{CO})_4$ , in contrast to the internal normalisation procedure that corrects for mass spectrometric and natural fractionation assuming an elemental Ni species.

The effects on mass-independent isotope measurements of prior Ni isotopic fractionation during the Mond process can be quantified. An anomaly produced in the internally normalised isotope ratio  $k/i$  by inappropriately corrected fractionation by the Mond processes will be given by the expression,

$$\epsilon^k \text{Ni}_i^j = 10 \delta^{j/i} \text{Ni} \left( \frac{\ln[(m_k + m_c)/(m_i + m_c)]}{\ln[(m_j + m_c)/(m_i + m_c)]} - \frac{\ln(m_k/m_i)}{\ln(m_j/m_i)} \right) \quad (3)$$

where isotope  $j$  and  $i$  are the normalising isotopes,  $m_c$  is the mass of  $(\text{CO})_4$ , and  $m_i$ ,  $m_j$  and  $m_k$  are the Ni isotopic masses.

Putting  $i = m_{61}$  and  $j = m_{58}$  and substituting

$$\delta^{58/61} \text{Ni} = (\delta^{60/58} \text{Ni}) \ln(m_{58}/m_{61}) / \ln(m_{60}/m_{58})$$

into Eq. (3) gives for  $k = m_{60}$ ,  $k = m_{62}$  and  $k = m_{64}$ , respectively,

$$\epsilon^{60}\text{Ni}_{61}^{38} = -0.054 \cdot \delta^{60/58} \text{Ni}$$

$$\epsilon^{62}\text{Ni}_{61}^{38} = 0.105 \cdot \delta^{60/58} \text{Ni}$$

$$\epsilon^{64}\text{Ni}_{61}^{38} = 0.459 \cdot \delta^{60/58} \text{Ni}$$

To illustrate these effects vectors have been plotted in Figs. 5 and 4 to simulate the effects of creating NIST SRM 986 from BSE Ni via the Mond process. As can be seen, the magnitude and sense of mass-independent isotopic differences are well explained by this mechanism. Industrially processed Ni must therefore be considered an arbitrary reference point, albeit, independently calibrated in the case of NIST SRM 986. Natural mass-dependent fractionation of Ni can also lead to subtle mass-independent anomalies as seen in the pentlandite PtYG. Thus the small mass-independent variability in terrestrial samples should not be unexpected.

The small but significant mass-independent variations in terrestrial materials, purified standards in particular, show that for inter-laboratory consistency at the highest precision a single, homogeneous reference material or standard must be used. This is currently not the case, as the studies of Quitté et al. (e.g. Quitté et al., 2006, 2010; Quitté and Oberli, 2006) use an Aldrich solution standard, Bizzarro et al. (e.g. Bizzarro et al., 2007; Bizzarro et al., 2010) reported their data relative to an ‘in-house’ standard whereas the work from Bristol (Regelous et al., 2008; Steele et al., 2010) and Chicago (e.g. Cook et al., 2006; Dauphas et al., 2008) use NIST SRM 986. Since NIST SRM 986 is from

a single, well characterised batch of Ni that can be obtained by all laboratories, we suggest that this is used as the primary reference standard.

An obvious alternative might be normalisation to Ni separated from a natural sample thought to be representative of bulk silicate Earth (BSE). This is similar to the  $\epsilon\text{Nd}_{\text{CHUR}}$  nomenclature that expresses  $^{143}\text{Nd}/^{144}\text{Nd}$  ratios relative to a chondritic composition (e.g. DePaolo and Wasserburg, 1976). Mantle peridotites, such as JP-1 measured in this study, ought to provide a good sample of BSE. It is straightforward to apply a simple numerical correction to place epsilon unit data normalised to a laboratory standard into BSE normalised space. Thus we also report our data, expressed relative to our best estimate of BSE from a weighted mean of JP-1 and DTS-2, in Table 3. This approach gives an aesthetically pleasing significance to an epsilon value of zero, i.e.  $\epsilon = 0 = \text{BSE}$ . However, the calculation of  $\epsilon$  units in this and the majority of MC-ICP-MS studies is largely an analytical tool to increase reproducibility. It is not a requirement that the composition of the normalising standard has scientific significance; it only acts as an arbitrary reference point. The use of natural materials as normalising standards may have several drawbacks, not least that it is not yet known which, if any, are truly representative of the Ni isotopic composition of BSE. Analysis of a wide variety of different terrestrial samples is required to define accurately and precisely the composition of the BSE. Until this has been done the exact ratio for this reference may change with time potentially producing a lack of consistency in data within the literature. Furthermore, high precision analyses, such as are reported here, require significant amounts of Ni ( $>10 \mu\text{g}$ ) and it thus makes sense to use a purified standard that does not need further processing. It is worth noting that the normalisation protocol adopted

here has been used for other systems with similar analytical concerns. For example  $^{142}\text{Nd}/^{144}\text{Nd}$  ratios are reported relative to a terrestrial standards rather than the traditional chondritic reference of  $^{143}\text{Nd}/^{144}\text{Nd}$  measurements. Therefore it seems justified to use a certified reference standard such as NIST SRM 986 as a normalising reference even though there is no specific significance of the zero in the resulting epsilon notation.

#### 4.2. Precision and reproducibility

Every sample in this study was measured at least four times during one analytical session and some samples were measured multiple times during multiple analytical sessions. So that all the data can be compared, deviations from the sample mean have been calculated by subtracting each sample mean from the corresponding measurements of the same sample. Therefore, for each sample, the mean of the deviations is zero and a single standard deviation (SD) can be calculated from the whole data set via  $s^2 = k^{-1} \sum_i d_i^2$ , where  $d_i$  are the deviations,  $s$  is the SD and  $k$  is the number of degrees of freedom equal to the difference between the number of analyses and the number of samples (Kenney and Keeping, 1951, Chapter, 7.11). The SD so calculated includes the reproducibility of every repeat measurement of every sample, and repeat dissolutions of standards (see below). An alternative method of assessing the external precision of a sample set could be based on repeat analyses of a solution standard. This is not as representative as it does not take into account potential sources of scatter such as any potential residual matrix in the samples affecting fractionation behaviour or contributing interferences or the effects of fractionation on ionic exchange columns.

Table 3

The same Ni isotopic data as in Table 2 re-normalised such that our best estimate of BSE = 0. The errors have been recalculated to include contributions from both the repeat measurements of the peridotite standards JP-1 and DTS-2 and the measurement of each individual sample.

Sample	Group	NHM No.	$n$	$n64$	$\epsilon^{60}\text{Ni}_{61}^{\text{r}}$	2 SE	$\epsilon^{62}\text{Ni}_{61}^{\text{r}}$	2 SE	$\epsilon^{64}\text{Ni}_{61}^{\text{r}}$	2 SE
<i>Iron meteorites</i>										
Tlacotepec	IVB	1959913	4	4	-0.130	0.020	-0.013	0.018	0.015	0.062
Santa Clara	IVB	1983,M27	16	4	-0.115	0.018	0.051	0.041	0.250	0.076
Hoba	IVB	1930976	8	8	-0.116	0.018	0.048	0.019	0.095	0.053
CoGH	IVB	1985,M246	4	4	-0.120	0.009	0.063	0.012	0.152	0.060
Skookum	IVB	—	4	4	-0.123	0.039	0.031	0.049	0.049	0.076
Putnam County	IVA	90228	8	8	-0.043	0.020	-0.105	0.034	-0.362	0.082
Bristol	IVA	1955226	16	8	-0.042	0.021	-0.083	0.028	-0.284	0.061
Bendegó	IC	66585	4	4	-0.007	0.020	-0.037	0.029	-0.149	0.078
Arispe	IC	86425	4	4	-0.043	0.027	-0.165	0.050	-0.436	0.094
Lenarto	IIIAB	61304	4	4	-0.041	0.030	-0.119	0.037	-0.437	0.115
Henbury	IIIAB	—	4	4	-0.050	0.025	-0.126	0.045	-0.423	0.050
Coahuila	IIAB	54242	4	4	-0.025	0.018	-0.124	0.041	-0.378	0.040
<i>Terrestrial standards</i>										
NIST SRM 361	T	—	72	41	-0.005	0.010	-0.007	0.016	0.017	0.039
NIST SRM 986-col	T	—	4	4	0.008	0.009	-0.060	0.030	-0.119	0.047
CPI	T	—	16	12	0.008	0.012	-0.019	0.019	-0.036	0.037
NiSalt	T	—	16	16	-0.010	0.011	0.022	0.021	0.107	0.052
PtYG	T	—	20	20	0.016	0.011	-0.045	0.020	-0.107	0.039
JP-1	T	—	58	50	0.000	0.010	0.000	0.014	-0.003	0.031
DTS-2	T	—	4	4	-0.001	0.033	0.002	0.064	0.042	0.102

Fig. 6 shows the deviations from sample mean, as described above, plotted in  $\epsilon^{60}\text{Ni}_{61}^{\text{SS}}$  vs.  $\epsilon^{62}\text{Ni}_{61}^{\text{SS}}$  and  $\epsilon^{62}\text{Ni}_{61}^{\text{SS}}$  vs.  $\epsilon^{64}\text{Ni}_{61}^{\text{SS}}$  space. We emphasise that the plots include the data from every analysis, from every sample in this study, excluding samples discounted for non-statistical reasons such as, the solution running out, or high Zn/Ni; no statistical rejection criteria have been used. The data set gives a 2 SD external precision of 0.056‰, 0.091‰ and 0.165‰ for  $\epsilon^{60}\text{Ni}_{61}^{\text{SS}}$ ,  $\epsilon^{62}\text{Ni}_{61}^{\text{SS}}$  and  $\epsilon^{64}\text{Ni}_{61}^{\text{SS}}$ , respectively, for an individual analysis.

The precision of individual samples has been assessed by determining the 2 SE of the mean of each sample; it is these errors that are reported in the data table and plotted in the figures. This error includes all repeats of a single sample, either measured in the same run, or between different runs on different days. The maximum 2 SE of the samples in this study are 0.038‰, 0.058‰ and 0.135‰ for  $\epsilon^{60}\text{Ni}_{61}^{\text{SS}}$ ,  $\epsilon^{62}\text{Ni}_{61}^{\text{SS}}$  and  $\epsilon^{64}\text{Ni}_{61}^{\text{SS}}$  ( $n = 4$ ), respectively, while they are typically 0.027‰, 0.045‰, and 0.081‰ for  $\epsilon^{60}\text{Ni}_{61}^{\text{SS}}$ ,  $\epsilon^{62}\text{Ni}_{61}^{\text{SS}}$  and  $\epsilon^{64}\text{Ni}_{61}^{\text{SS}}$  ( $n = 4$ ), respectively.

Our sample set also includes six repeat of NIST SRM 361 and four of JP-1. These repeat dissolutions can be used to assess the reproducibility of the full chemical separation procedure. Every analysis of the two standards are shown in Fig. 7. There are fewer  $\epsilon^{64}\text{Ni}_{61}^{\text{SS}}$  analyses due to the occurrence of some analytical sessions with high Zn/Ni ratios early in the study. Firstly, data in Fig. 7 show that there is no significant bias introduced when the same sample is re-dissolved and processed through chemical separation multiple times. Secondly, JP-1 comprises 54 repeat measurements and has 2 SD of 0.06‰, 0.07‰ and 0.15‰ for  $\epsilon^{60}\text{Ni}_{61}^{\text{SS}}$ ,  $\epsilon^{62}\text{Ni}_{61}^{\text{SS}}$  and  $\epsilon^{64}\text{Ni}_{61}^{\text{SS}}$ , respectively. These estimates of the 2 SD error are the same within error as those estimated from the data set as a whole (Fig. 6). This suggests

that the reproducibility of our dissolutions and chemical separation protocol is high and does not constitute a secondary source of uncertainty on top of the mass-spectrometric procedure.

Internal errors, i.e. the standard error based on 100 cycles of integration comprising one analysis, have not been reported here because of a measurement artefact that decreases the apparent cycle-to-cycle reproducibility. This artefact arises from the differing responses of amplifiers fitted with  $10^{10} \Omega$  vs.  $10^{11} \Omega$  feedback resistors. The integrated beam intensity for each cycle is the convolution of the input signal, the amplifier response, and a boxcar function representing the integration time. Hence, the different amplifier responses result in imperfect measurement ‘tracking’ of two signals with identical beam noise and the observed reduction in cycle-to-cycle reproducibility. However, assuming there is no ‘lost’ time between cycles, on average a high ratio of the two measured beams resulting from a sudden signal change near the end of one cycle will be accompanied by a low ratio in the next, i.e. this tracking noise is not random and will cancel out in the mean ratio reported for an analysis.

#### 4.3. Effects of possible residual interferences

Regelous et al. (2008), Dauphas et al. (2008) and Chen et al. (2009) suggested that the range in Ni isotope data of Bizzarro et al. (2007) could be accounted for by a small variable interferences on mass 61, the least abundant Ni isotope they measured. Chen et al. (2009) noted that they had problems obtaining reproducible Ni isotope data using MC-ICP-MS and argued that this might be due to unspecified interferences. Our high precision peak flat determinations reported in Fig. 1, however, demonstrate there are no discernible molecular interferences that contribute to the ratios at greater than 0.1‰ level. Only the NiH

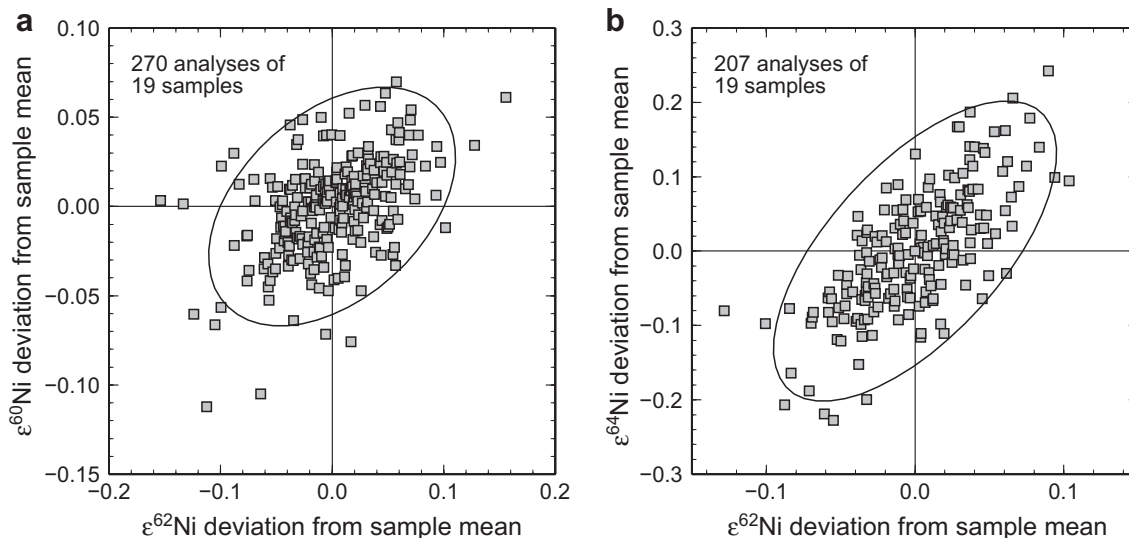


Fig. 6. Plots of deviations from sample means. The data were created by subtracting the mean of individual samples from every measurement of that sample. This has the effect of normalising the mean of the deviations to be zero so they can be compared as a single data set. Error ellipses are 95% confidence. This gives the 2 SD external precision on one analysis of 0.055‰, 0.090‰ and 0.165‰ for  $\epsilon^{60}\text{Ni}_{61}^{\text{SS}}$ ,  $\epsilon^{62}\text{Ni}_{61}^{\text{SS}}$  and  $\epsilon^{64}\text{Ni}_{61}^{\text{SS}}$ , respectively. All samples are the average of at least four repeats, thus the expected standard error is 0.5 times the 2 SD.

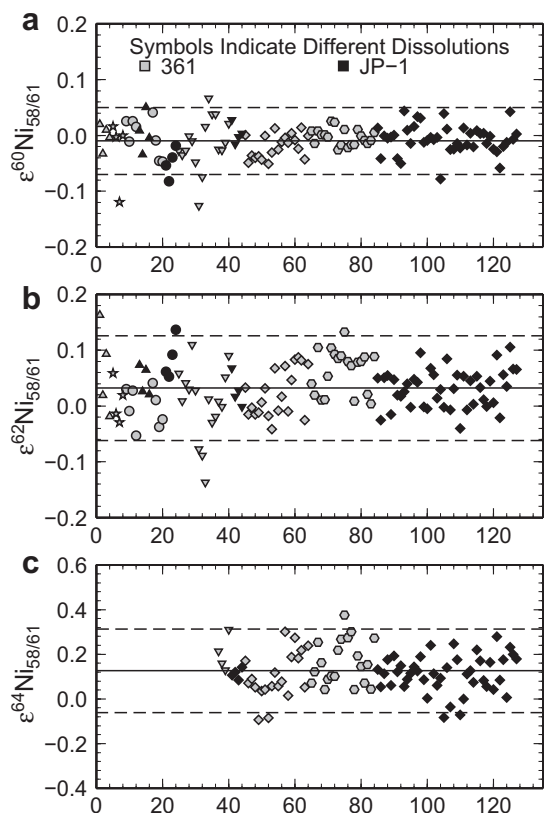


Fig. 7. Plots showing the spread of individual analyses of the two standards JP-1 and NIST SRM 361 from different dissolutions. These standards are plotted because they require full chemical separation so are used to investigate any bias introduced by this processing. Black symbols indicate JP-1 analyses while grey symbols show NIST SRM 361. The different symbols correspond to different dissolutions. The plots show there is no significant bias between the same samples processed through chemistry during different batches. The solid lines indicate the average of all measurements and the dashed lines display 2 SD.

interferences are not resolved, and these should be readily corrected by the external normalisation to bracketing Ni standards, see Section 2.4.1. Since these peak flat measurements were made on standards, however, we should also investigate the systematics of our data on the iron meteorites for any potential role of sample-related interferences. A significant observation in this regard is the good agreement between samples measured by our new analytical procedure and those previously reported in Regelous et al. (2008) (see Fig. 9 and Section 4.6). As detailed earlier (Section 2.4.1), we currently resolve interferences at  $M/\Delta M \geq 6000$  for all collected masses, whereas in Regelous et al. (2008), only the Faraday cup collecting mass 62 was set to exploit this high resolution. The latter approach was taken for convenience given the absence of observed interferences in masses other than 62. In this study, however, we adopted a more cautious protocol and resolved potential molecular interferences on all masses. Hence we suggest that molecular interferences are not a major control on the Ni isotopic variability in these iron meteorites.

We can also explore more generally the effects of hypothetical interferences on Ni isotope ratios. A key point is

that some iron meteorites have  $\epsilon^{60}\text{Ni}_{61}^{\text{ss}}$ ,  $\epsilon^{62}\text{Ni}_{61}^{\text{ss}}$  and  $\epsilon^{64}\text{Ni}_{61}^{\text{ss}}$  lower than the terrestrial reference. This is also true of the  $\epsilon^{60}\text{Ni}_{61}^{\text{ss}}$  and  $\epsilon^{62}\text{Ni}_{61}^{\text{ss}}$  of the chondrite data of Regelous et al. (2008). In our normalisation scheme, interferences on masses 60, 62 and 64 can only act to increase the ratios  $^{60}\text{Ni}/^{61}\text{Ni}$ ,  $^{62}\text{Ni}/^{61}\text{Ni}$  and  $^{64}\text{Ni}/^{61}\text{Ni}$ , respectively. The effects of interferences on masses 58 and 61 are more complex as they propagate into all isotopic ratios as a result of internal normalisation and are illustrated in Fig. 8. Therefore, if such interferences were important they should result in coupled variability in both Fig. 8(a) and (b). This is not observed. A mass 61 interference cannot reproduce the array of meteorite data in Fig. 8(b) as a result of perturbation of a terrestrial ratio. While every precaution is taken against the possibility of contamination: spike separations are carried out in a separate laboratory using separate materials, spikes are analysed on a separate instrument, it is important to consider the possibility of a non-natural blank. The trajectories of spike addition of the spike is on the low abundance  $^{61}\text{Ni}$  isotope, and the trajectories broadly follow those of a  $^{61}\text{Ni}$  interference. Therefore, the possibility of spike contamination is unlikely for the reasons cited above.

Superficially of more concern is that the meteorite data lie on a line with slope 3 in Fig. 8(b), which could be explained by an uncorrected interference on mass 58. Yet the Ni isotope ratios are both higher and lower than the terrestrial reference. If such variability were an artefact imposed on uniform terrestrial compositions, then some samples would require an interference on mass 58 and others a deficit. This could possibly be explained by insufficient and excess correction of a  $^{58}\text{Fe}$  interference, respectively. The latter could potentially result from scattering of  $^{40}\text{Ar}^{16}\text{O}$  onto the  $^{56}\text{Fe}$  beam used to monitor Fe during analysis. Two important considerations, however, demonstrate that this elaborate scenario is implausible. Firstly, the meteorite Ni isotope data do not plot along a trajectory equivalent to a 58 deficit vector (labelled  $^{40}\text{Ar}^{16}\text{O}^+$ ) in Fig. 8(a). Thus, at worst, it might be argued that there is scope for a  $^{58}\text{Ni}$  interference to account for some of the IVB meteorites in both Fig. 8(a) and (b). The second issue however, is the magnitude of the interference required. In order to generate the composition of the IVB irons from a terrestrial composition, an uncorrected  $^{58}\text{Fe}$  contribution equivalent to an Fe/Ni ratios of  $9 \times 10^{-3}$  would be required (Fig. 8). However, Fe/Ni ratios of all sample were measured, and corrected by peak stripping, during analysis of each sample (see Section 2.4.2). Measured Fe/Ni ratios are  $<1 \times 10^{-4}$  normally  $<3 \times 10^{-5}$ , in the worst case almost two orders of magnitude lower than those required to account for the anomaly in the IVB irons, even if no interference correction was applied.

Thus, we feel we have extensively addressed the possibility of interferences affecting our data and find no significant influence.

#### 4.4. Nuclear field shift effects

It has been suggested (Fujii et al., 2006, 2009) that mass-independent anomalies may be the result of mass-independent fractionation controlled by the nuclear field shift effect

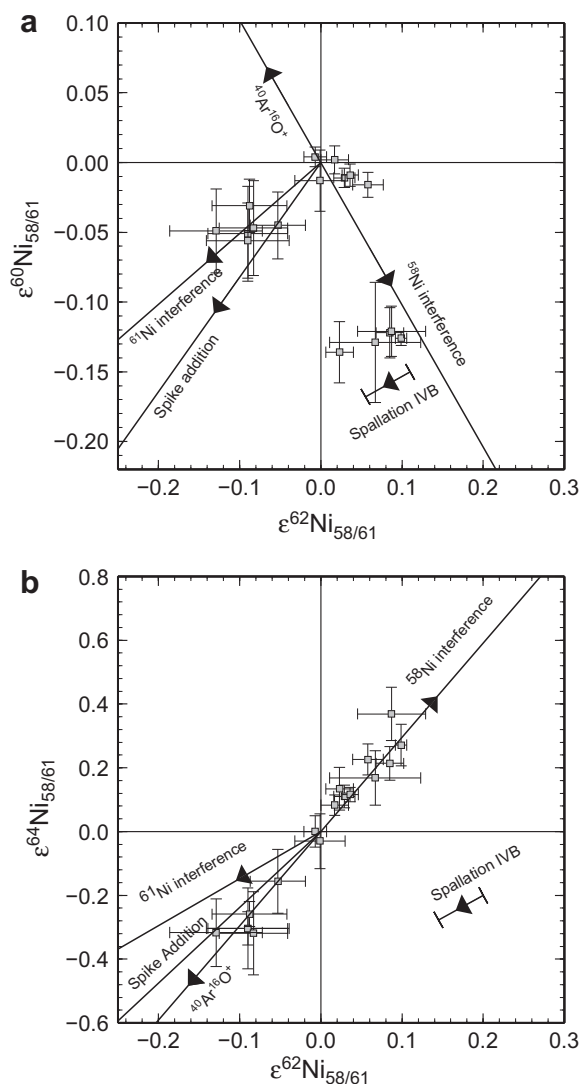


Fig. 8. Plots showing the trajectories in Ni isotope space of interferences on the normalising isotopes. They have been propagated through the mass bias correction to include contributions from the normalising isotopes. Also shown is the trajectory and magnitude of maximum spallation of a IVB iron meteorite, with an exposure age of 1 Ga, see Table 4. Some iron meteorites and all chondrites will have been considerably less affected due to their younger exposure ages.

(Bigeisen, 1996) and not result from mixing of material from different stellar sources. The nuclear field shift effect is concerned with non-mass-dependent fractionation between isotopes resulting from nuclear size. It will typically manifest as mass-independent anomalies between odd-even isotopes. Nickel has only one odd mass isotope,  $^{61}\text{Ni}$ , and since this study uses  $^{58}\text{Ni}/^{61}\text{Ni}$  as a normalising ratio this effect could propagate into all the data. Such an influence on  $^{61}\text{Ni}$ , however, will appear as a perturbation along the same trajectory as an interference on  $^{61}\text{Ni}$ , Fig. 8. Therefore, by the same reasoning used to show a  $^{61}\text{Ni}$  interference is not present (Section 4.3), we have already shown that the

nuclear field shift effect does not have a significant effect on our data.

#### 4.5. Cosmic ray spallation

As stated above, we chose iron meteorites for this study because they do not contain refractory components and so selective dissolution problems should be negligible. However, in general, iron meteorites have longer cosmic ray exposure ages than the chondrites so we need to consider the possible perturbations due to spallation reactions. We have investigated this with numerical modelling of spallation effects.

Galactic cosmic ray (GCR) induced spallation effects on meteoroids were modelled using the MCNPX (Monte Carlo N Particle eXtended) code version 2.5.0 (Pelowitz, 2005). Transport of protons, neutrons, and pions (and all their antiparticles) is considered. Tabulated excitation functions were used as far as possible and the Bertini model (the MCNPX default) used where no tabulated data are provided (proton data for C,  $^{58}\text{Fe}$ , and Co). The computer codes were used to predict the differential neutron flux in spherical iron meteoroids from which were calculated  $(n, \gamma)$  reaction rates for various nuclides. The default  $(n, \gamma)$  excitation functions packaged with the MCNPX distribution were used to calculate reaction rates for all elements except Ca, where we used the Japanese Evaluated Nuclear Data Library (JENDL 3.3) for better resolution in the resonance region. See discussion by Kollár et al. (2006). The GCR parameterisation follows Masarik and Reedy (1994) with the solar modulation parameter  $\Phi = 650$  MeV. The effective proton flux was normalised to the  $^{41}\text{Ca}$  activity depth profile in the Apollo 15 lunar drill core and adjusted for the difference between GCR flux at lunar compared to meteoroid orbits. See Kollár et al. (2006) for details of this normalisation scheme.

The effect on Ni target nuclei is dominated by capture of low energy (thermal or epithermal) neutrons whose flux peaks at some depth within a meteoroid. We have modelled meteoroids as spheres with radii chosen to approximately maximise the spallogenic perturbation of Ni isotopes near their centres. Thus, the spallation effects on Ni reported here should be considered upper limits. We took meteoroids with compositions corresponding to two irons: group IVB with density  $8.0\text{ g cm}^{-3}$ , radius 0.5 m and composition (by weight) Fe 83%, Ni 16.2%, Co 0.76%, P 0.045% and C 0.0045%, and group IC with density  $8.0\text{ g cm}^{-3}$ , radius 0.5 m and composition Fe 92.647%, Ni 6.64%, Co 0.465%, P 0.215% and C 0.016%. The  $(n, \gamma)$  reaction rates for all Ni and Co isotopes are considered in calculating the effect on the bulk Ni isotopic composition. Relative changes to Ni isotope abundances in parts per ten thousand for both the group IVB and IC compositions for an exposure age of 1 Ga are shown in Table 4. The largest effect is on  $^{61}\text{Ni}$  because of the capture on the more abundant  $^{60}\text{Ni}$  which has a collateral effect on all the other ratios through normalisation (Table 4).

The effect of spallation on normalised Ni isotopes predicted by this models is shown in Fig. 8(a) and (b) by vectors indicating the maximum possible perturbation. Note

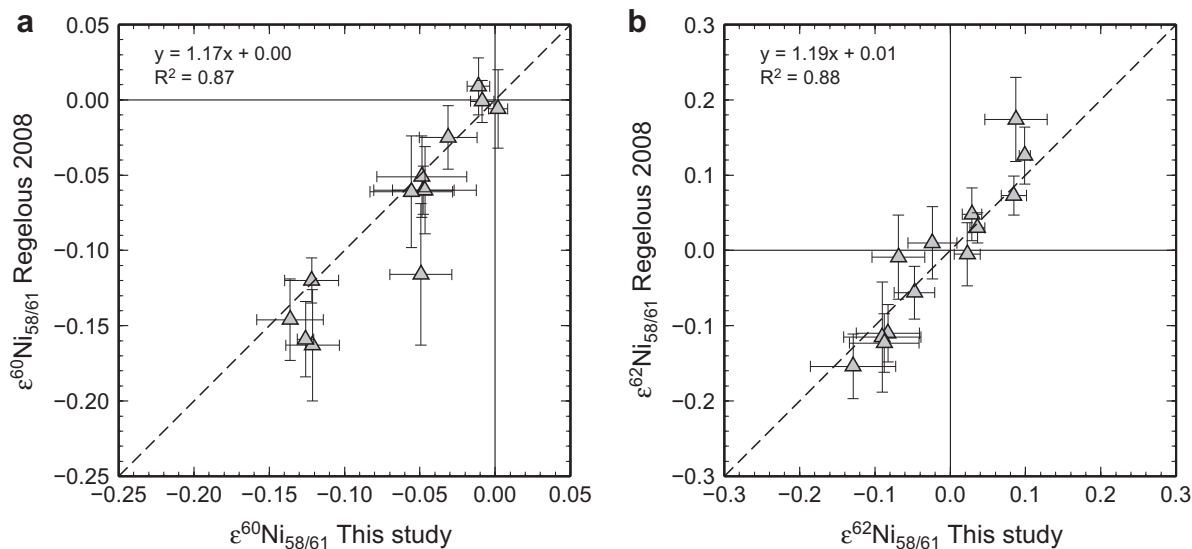


Fig. 9. Figure showing the good correlation between  $\epsilon^{60}\text{Ni}_{58/61}$  and  $\epsilon^{62}\text{Ni}_{58/61}$  collected during this study and that of [Regelous et al. \(2008\)](#), a previous study carried out in Bristol on many of the same samples.

that the spallation effect is small compared to the magnitude of isotopic anomalies we report. However, the small displacement of Tlacotepec from the other IVBs could be a spallation effect but the difference between the two ICs (Bendegó and Arispe) cannot be accounted for this way. In order to critically assess whether spallation alone can account for the Tlacotepec Ni data relative to the other IVBs both the exposure age and sample depth (pre-atmospheric distance below the surface) are required. In the case of our samples the depth is not known so we can only say that the discrepancy is plausibly a spallation effect. The exposure ages are ([Voshage and Feldmann, 1978](#)): Tlacotepec 945 Ma, Skookum 945 Ma, Cape of Good Hope 775 Ma and Hoba 340 Ma.

#### 4.6. Comparison with published data

Previous studies have investigated mass-independent Ni isotopic anomalies in bulk meteorites and debate continues as to the existence of anomalies. Varying levels of precision have been achieved by previous studies, as plotted in [Fig. 10](#) in comparison with the range of anomalies reported by [Regelous et al. \(2008\)](#). [Fig. 10](#) shows that assuming a total range in  $\epsilon^{62}\text{Ni}_{58/61}$  of  $0.4\text{‰}$ , only two other studies ([Dauphas et al., 2008](#); [Regelous et al., 2008](#)) have the precision to resolve bulk sample anomalies from terrestrial ratios. This may account for much of the debate concerning the existence of anomalies. Case by case we discuss in more detail a comparison with selected studies that highlight particular view points within the literature.

As discussed above, [Fig. 9](#) compares data from this study with that of ([Regelous et al., 2008](#)). Data from [Regelous et al. \(2008\)](#) were measured on the same instrument (Neptune 1 at Bristol), but was obtained using a different mass-spectrometric procedure and slightly different chemistry, i.e. without an extra column to remove Zn. As can be seen from [Fig. 9](#), data from this study collected on the same

samples show good agreement with the data from [Regelous et al. \(2008\)](#) and are within external error in both  $\epsilon^{60}\text{Ni}_{58/61}$  and  $\epsilon^{62}\text{Ni}_{58/61}$ .

[Bizzarro et al. \(2007\)](#) conducted a study of  $\epsilon^{60}\text{Ni}_{58/61}$  in early Solar System bulk samples. As has been noted above and by other studies ([Dauphas et al., 2008](#); [Regelous et al., 2008](#); [Chen et al., 2009](#)), the variability of the data from [Bizzarro et al. \(2007\)](#) is consistent with an interference on  $^{61}\text{Ni}$ , one of the normalising isotopes. One sample, Skookum (IVB iron), was kindly provided to us as a separated Ni solution by Martin Bizzarro for comparison. [Bizzarro et al. \(2007\)](#) reported  $-0.274 \pm 0.077$  and  $-0.366 \pm 0.135$   $\epsilon^{60}\text{Ni}_{58/61}$  and  $\epsilon^{62}\text{Ni}_{58/61}$ , respectively, for this solution but, our analysis of the same solution, after anionic exchange Zn cleanup column,<sup>1</sup> yielded  $-0.129 \pm 0.043$  and  $0.067 \pm 0.056$  for  $\epsilon^{60}\text{Ni}_{58/61}$  and  $\epsilon^{62}\text{Ni}_{58/61}$ , respectively. The latter ratios agree well with our other analyses of IVB irons, despite the different Ni separation protocol and larger Fe correction. This supports the previous suggestions that the Copenhagen measurements are likely compromised by an instrumental artefact, such as an interference on mass 61.

A study of meteoritic metal from irons and chondrites was undertaken by [Cook et al. \(2006\)](#), who were the first to report  $\epsilon^{64}\text{Ni}_{58/61}$  in bulk samples. The external precision they report for  $\epsilon^{64}\text{Ni}_{58/61}$  is  $1.5\text{‰}$  2 SE, which is an order of magnitude less precise than our data. The data reported by [Cook et al. \(2006\)](#) and a subsequent paper [Cook et al. \(2008\)](#) are entirely consistent with our data, but at lower precision, which resulted in them finding no resolvable anomalies for Ni isotopes in bulk iron and chondritic metal samples.

<sup>1</sup> In order to obtain maximum separation of Zn from Ni, 1 M HCl was used. Under these conditions Fe is not retained on the resin.

Table 4

Upper limit of the effect on Ni isotopes in parts per ten thousand on the relative isotopic abundance and the normalised ratios,  $\epsilon^i\text{Ni}_{61}^{188}$ , resulting from 1 Ga exposure to galactic cosmic rays.

<i>i</i>	Relative $^i\text{Ni}$ abundance change (‰)		Spallogenic change in $\epsilon^i\text{Ni}_{61}^{188}$	
	IVB	IC	IVB	IC
$^{58}\text{Ni}$	−0.002	−0.002	—	—
$^{60}\text{Ni}$	+0.007	+0.010	−0.018	−0.012
$^{61}\text{Ni}$	+0.038	+0.034	—	—
$^{62}\text{Ni}$	−0.004	−0.003	−0.055	−0.048
$^{64}\text{Ni}$	−0.001	−0.001	−0.077	−0.069

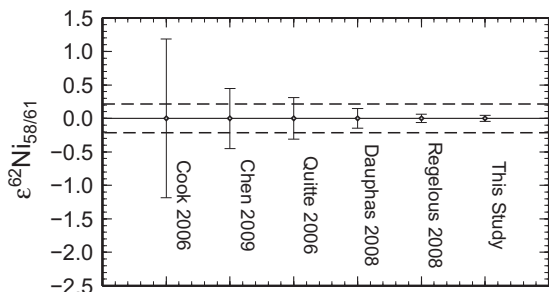


Fig. 10. Plot showing comparison between average error in  $\epsilon^{62}\text{Ni}_{61}$  (2 SE) from various other recent Ni isotope cosmochemical studies (Cook et al., 2006; Quitté et al., 2006; Dauphas et al., 2008; Chen et al., 2009) and this study. For comparison dashed lines indicate the range in  $\epsilon^{62}\text{Ni}_{61}$  reported by Regelous et al. (2008). The errors from all studies have been adjusted to be equivalent to the  $^{58}\text{Ni}/^{61}\text{Ni}$  normalisation. Where studies (e.g. Quitté et al., 2006) quoted 2 SD we have calculated 2 SE to make them comparable. This comparison shows that few previous studies have had high enough precision to resolve anomalies.

Chen et al. (2009) concluded “the numerous atomic and molecular mass interferences for analysis of Ni by MC-ICP-MS present a serious analytical concern” so instead performed a study by multiple-collector, positive ion thermal ionisation mass spectrometry (MC-PTIMS). As discussed above (Section 2.4.2), we have overcome the ‘atomic interferences’ by chemical separation and quantitative interference correction and demonstrated that they make no significant contribution to the data. We further resolve the obvious molecular interferences, and see no evidence for other species other than minor NiH which is corrected by secondary normalisation (see Section 2.4.1). Therefore, we conclude that the limited precision achievable for Ni isotopes by MC-PTIMS, due to the difficulties in obtaining sufficiently intense ion beams, is a more limiting analytical problem.

Dauphas et al. (2008) conducted a high precision Ni and Fe isotope study of meteoritic materials and argued against the existence of anomalies. Their Ni isotope data are plotted in bold in Fig. 11, superimposed over the data reported in this study. Notably, these data sets are quite consistent with each other. It is more difficult to discern the correlated isotopic variations within the Dauphas et al. (2008) data as its precision is lower and only a limited range of meteorite types were analysed. Notably Dauphas et al. (2008) do not report data for the carbonaceous chondrites (CC)s or IVB

irons, the groups which show the largest anomalies in this study and Regelous et al. (2008).

#### 4.7. Nucleosynthetic implications

Planetary differentiation processes on iron meteorite parent bodies should have efficiently homogenised refractory pre-solar grains observed in chondrites that contain extreme isotope ratios. Therefore, the anomalies we observe in iron meteorites should result from planetary scale heterogeneity and not from selective dissolution during analysis. Moreover, the slope in  $\epsilon^{64}\text{Ni}_{61}$  against  $\epsilon^{62}\text{Ni}_{61}$  from this study yields,  $\sim 3$ , is within error of the slope produced by a regression of early measurements of refractory inclusions through terrestrial ratios (Birck and Lugmair, 1988). The similarity between the slopes in  $\epsilon^{64}\text{Ni}_{61}$  against  $\epsilon^{62}\text{Ni}_{61}$  yielded by iron meteorites and refractory inclusions implies the anomalies have a common history, therefore, supports the suggestion that the correlation reflects some earlier nebular heterogeneity inherited by iron meteorite parent bodies.

The neutron-rich character of  $^{62}\text{Ni}$  and  $^{64}\text{Ni}$  requires their production in a neutron-rich nucleosynthetic environment (Burbidge et al., 1957). Indeed it has been noted that correlated  $\epsilon^{50}\text{Ti}_{49}$ ,  $\epsilon^{54}\text{Cr}_{52}$  and  $\epsilon^{62}\text{Ni}_{61}$  have been observed in refractory inclusions (Birck and Lugmair, 1988; Niederer et al., 1980; Niemeyer and Lugmair, 1981) and bulk sample chondrites (Niemeyer, 1985; Trinquier et al., 2007; Leya et al., 2008; Regelous et al., 2008; Trinquier et al., 2009), is evidence for their common genesis (Regelous et al., 2008; Leya et al., 2009). Recent studies, (Dauphas et al., 2010; Qin et al., 2010), reported analyses of nano-particles with highly anomalous  $\epsilon^{54}\text{Cr}_{52}$ ; a strong candidate for the carrier of Cr isotope anomalies in meteorites. It has previously been suggested that the source for heterogeneity in neutron-rich Fe-peak isotopes in the early Solar System might be heterogeneous input from a SN Ia (Timmes et al., 1995; Woosley, 1997). Therefore, the correlation between  $\epsilon^{62}\text{Ni}_{61}$  and  $\epsilon^{64}\text{Ni}_{61}$  is consistent with heterogeneous distribution of material from an SN Ia. However, SN Ia are rare events not thought to be associated with star forming regions, therefore, these signatures may be much older than the Solar System and were released from the previously homogenised interstellar medium (ISM) by subsequent processing within the Solar System (e.g. Trinquier et al., 2009). The spinel nano-particles found by Dauphas et al. (2010) are not likely to contain significant amounts

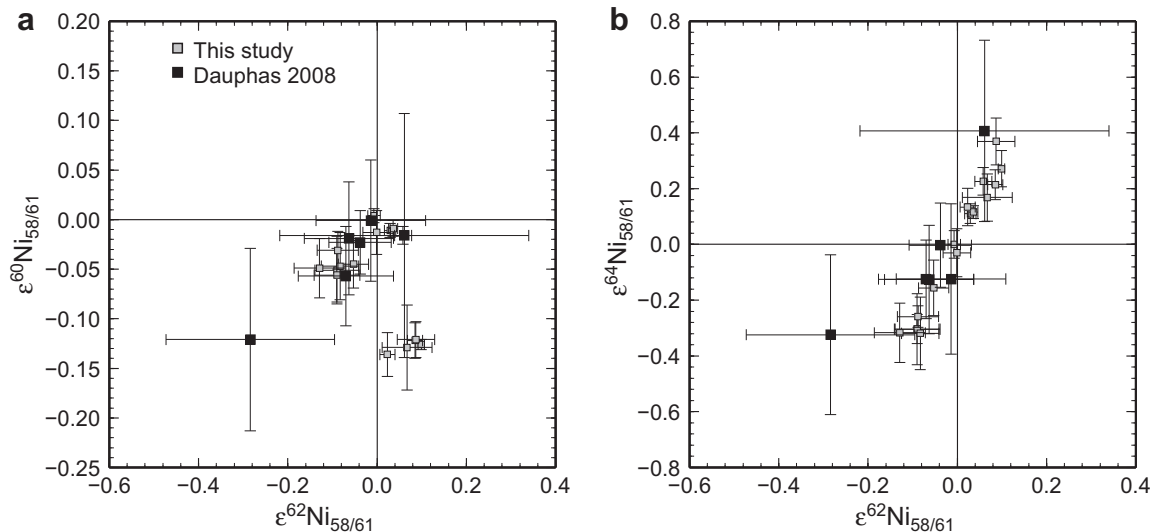


Fig. 11. Plots showing comparison between data from Dauphas et al. (2008) and this study. They show that our more precise data are entirely consistent with data from the previous study, but with the higher precision we achieve, we are able to define clear correlations.

of Ni thus are unlikely to be the carrier responsible for Ni isotope heterogeneity in meteorites. However, the ultimate source of  $^{54}\text{Cr}$  anomalies is likely to be the same source as that of the Ni isotope anomalies. Anomalies in  $^{64}\text{Ni}$  are of particular significance because the extreme neutron enrichment of this isotope means it can only be produced in highly neutron-rich environments. Neutron-rich isotopes like  $^{64}\text{Ni}$  and  $^{54}\text{Cr}$  are likely to be provided to the Solar System by supernova input, which may also provide its inventory of short-lived radionuclides (SLR). Dauphas et al. (2010) suggest the O/Ne–O/C zones of a type II supernovae (SN II) are the most likely source of the  $^{54}\text{Cr}$  anomalous grains they measured, but cannot rule out input from an SN Ia. That there is no correlation of  $\epsilon^{64}\text{Ni}_{58/61}$  or  $\epsilon^{62}\text{Ni}_{58/61}$  with  $\epsilon^{60}\text{Ni}_{58/61}$  suggests there is another control on the variation in  $\epsilon^{60}\text{Ni}_{58/61}$ , possibly differential input of a component rich in live or fossil  $^{60}\text{Fe}$ .

It is interesting that the iron meteorite analyses from this study, and those reported in Regelous et al. (2008), cover much of the same range as the chondrites previously analysed by Regelous et al. (2008). Therefore, the similarity of the range of iron meteorites with that of chondrites suggests that the protolith material of iron meteorites is represented by only one or two chondrite groups. If they were formed by accretion of material from more chondrite groups they would yield much more homogenous Ni isotopic anomalies, though not necessarily around terrestrial ratios. This finding could be consistent with radial heterogeneity in the early Solar System, with parent bodies at the same heliocentric distance inheriting the same inventory of precursor material.

## 5. SUMMARY

We have built on the procedure of Regelous et al. (2008) to improve precision and include measurement of  $^{64}\text{Ni}$ , the least abundant stable Ni isotope. The measurement preci-

sion of a typical sample, consisting of four repeat measurements, is  $0.027\text{‰}$ ,  $0.045\text{‰}$  and  $0.081\text{‰}$  (2 SE) for  $\epsilon^{60}\text{Ni}_{58/61}$ ,  $\epsilon^{62}\text{Ni}_{58/61}$  and  $\epsilon^{64}\text{Ni}_{58/61}$ , respectively. With this increased precision we have been able to resolve small ( $\lesssim 0.1\text{‰}$ ) differences between a variety of terrestrial materials. These differences, as suggested by Young et al. (2002), may be expected from the correction of all fractionation processes using a single, exponential (kinetic) law and atomic masses. Data from peridotites, which probably best represent the composition of Ni in the BSE, are offset from NIST SRM 986 by  $-0.006\text{‰}$ ,  $0.036\text{‰}$  and  $0.119\text{‰}$  in  $\epsilon^{60}\text{Ni}_{58/61}$ ,  $\epsilon^{62}\text{Ni}_{58/61}$  and  $\epsilon^{64}\text{Ni}_{58/61}$ , respectively.

Our new data for iron meteorites show a total range of  $0.14\text{‰}$ ,  $0.23\text{‰}$  and  $0.69\text{‰}$  for  $\epsilon^{60}\text{Ni}_{58/61}$ ,  $\epsilon^{62}\text{Ni}_{58/61}$  and  $\epsilon^{64}\text{Ni}_{58/61}$ , respectively. All of the meteoritic samples analysed in this study are resolvable from bulk terrestrial Ni in at least one Ni isotope ratio.

We have assessed our data for analytical artefacts due to: interferences, residual non-exponential machine induced mass-dependent fractionation, residual natural mass-dependent fractionation due to a different law or fractionation as a different mass, the nuclear field shift effect and cosmic ray spallation. We find that none of these processes can account for the compositions we report in iron meteorites. Instead the positive correlation of  $\epsilon^{64}\text{Ni}_{58/61}$  against  $\epsilon^{62}\text{Ni}_{58/61}$  is consistent with heterogeneous input from a SN Ia, however, the lack of correlation with  $\epsilon^{60}\text{Ni}_{58/61}$  requires a different origin for the  $^{60}\text{Ni}$  variation.

## ACKNOWLEDGEMENTS

We thank Derek Vance (BIG), Vyllinniskii Cameron (BIG) and Matthias Willbold (BIG) for their helpful advice, discussion and suggestions; Sara Russell (NHM) and Caroline Smith (NHM) for discussion and meteorite samples; Rich Beckley (AusQuest) and

Martin Gole (BHP Billiton) for providing the sample PtYG; and NERC (NE/F007329/1), STFC (ST/F002734/1) and NHM for funding this work. We are grateful to three anonymous reviewers for their helpful comments which improved the manuscript. We thank Dimitri Papanastassiou for his editorial handling and for his thorough and spirited discussion. We also thank Rich Walker, Shichun Huang, Fred Moynier, Steve Shirey and Yuri Amelin for their comments on normalisation issues. Finally we would like to thank Frank Podosek for his resourceful editorial handling.

## REFERENCES

- Andreasen R. and Sharma M. (2007) Mixing and homogenization in the early Solar System: clues from Sr, Ba, Nd, and Sm isotopes in meteorites. *Astrophys. J.* **665**, 874–883.
- Bigeleisen J. (1949) The relative reaction velocities of isotopic molecules. *J. Chem. Phys.* **17**, 675–678.
- Bigeleisen J. (1996) Nuclear size and shape effects in chemical reactions. Isotope chemistry of the heavy elements. *J. Am. Chem. Soc.* **118**, 3676–3680.
- Bigeleisen J. and Mayer M. (1947) Calculation of equilibrium constants for isotopic exchange reactions. *J. Chem. Phys.* **15**, 261–267.
- Birck J. L. and Allègre C. J. (1984) Chromium isotopic anomalies in Allende refractory inclusions. *Geophys. Res. Lett.* **11**, 943–946.
- Birck J. L. and Lugmair G. W. (1988) Nickel and chromium isotopes in Allende inclusions. *Earth Planet. Sci. Lett.* **90**, 131–143.
- Bizzarro M., Ulfbeck D., Boyd J. A. and Haack H. (2010) Nickel isotope anomalies in iron meteorites. *Meteorit. Planet. Sci. Suppl.* **73**, 5161.
- Bizzarro M., Ulfbeck D., Trinquier A., Thrane K., Connelly J. and Meyer B. (2007) Evidence for a late supernova injection of <sup>60</sup>Fe into the protoplanetary disk. *Science* **316**, 1178–1181.
- Burbidge E. M., Burbidge G. R., Fowler W. A. and Hoyle F. (1957) Synthesis of the elements in stars. *Rev. Mod. Phys.* **29**, 547–650.
- Cameron V., Vance D., Archer C. and House C. H. (2009) A biomarker based on the stable isotopes of nickel. *Proc. Natl. Acad. Sci. USA* **106**, 10944–10948.
- Carlson R., Boyet M. and Horan M. (2007) Chondrite barium, neodymium and samarium isotopic heterogeneity and early Earth differentiation. *Science* **316**, 1175–1178.
- Chen J. H., Papanastassiou D. A. and Wasserburg G. J. (2009) A search for nickel isotopic anomalies in iron meteorites and chondrites. *Geochim. Cosmochim. Acta* **73**, 1461–1471.
- Cook D. L., Clayton R. N., Wadhwa M., Janney P. E. and Davis A. M. (2008) Nickel isotopic anomalies in troilite from iron meteorites. *Geophys. Res. Lett.* **35**, L01203.
- Cook D. L., Wadhwa M., Janney P. E., Dauphas N., Clayton R. N. and Davis A. M. (2006) High precision measurements of non-mass-dependent effects in nickel isotopes in meteoritic metal via multicollector ICPMS. *Anal. Chem.* **78**, 8477–8484.
- Dauphas N., Cook D. L., Sacrabany A., Fröhlich C., Davis A. M., Wadhwa M., Pourmand A., Rauscher T. and Gallino R. (2008) Iron 60 evidence for early injection and efficient mixing of stellar debris in the protosolar nebula. *Astrophys. J.* **686**, 560–569.
- Dauphas N., Remusat L., Chen J. H., Roskosz M., Papanastassiou D. A., Stodolna J., Guan Y., Ma C. and Eiler J. M. (2010) Neutron-rich chromium isotope anomalies in supernova nanoparticles. *Astrophys. J.* **720**, 1577–1591.
- DePaolo D. J. and Wasserburg G. J. (1976) Nd isotopic variations and petrogenetic models. *Geophys. Res. Lett.* **3**, 249–252.
- Dowling S. E. and Hill R. E. T. (1998) Komatiite-hosted Ni sulphide deposits, Australia. *J. Aust. Geol. Geophys.* **17**, 121–127.
- Fujii T., Moynier F. and Albarède F. (2006) Nuclear field vs. nucleosynthetic effects as cause of isotopic anomalies in the early Solar System. *Earth Planet. Sci. Lett.* **247**, 1–9.
- Fujii T., Moynier F. and Albarède F. (2009) The nuclear field shift effect in chemical exchange reactions. *Chem. Geol.* **267**, 139–156.
- Godycki L. E. and Rundle R. E. (1953) The structure of nickel dimethylglyoxime. *Acta Crystallogr.* **6**, 487–495.
- Gramlich J. W., Machlan L. A., Barnes I. L. and Paulsen P. J. (1989a) Absolute isotopic abundance ratios and atomic weight of a reference sample of nickel. *J. Res. NIST* **94**, 347–356.
- Gramlich J. W., Machlan L. A., Barnes I. L. and Paulsen P. J. (1989b) The absolute isotopic composition and atomic weight of terrestrial nickel. *J. Res. NIST* **94**, 357–362.
- Hartmann D., Woosley S. E. and El Eid M. F. (1985) Nucleosynthesis in neutron-rich supernova ejecta. *Astrophys. J.* **297**, 837–845.
- Heydegger H. R., Foster J. J. and Compston W. (1979) Evidence of a new isotopic anomaly from titanium isotopic ratios in meteoric materials. *Nature* **278**, 704–707.
- Hidaka H., Ohta Y. and Yoneda S. (2003) Nucleosynthetic components of the early Solar System inferred from Ba isotopic compositions in carbonaceous chondrites. *Earth Planet. Sci. Lett.* **214**, 455–466.
- Imai N., Terashima S., Itoh S. and Ando A. (1995) 1994 compilation values for GSJ reference samples, “Igneous rock series”. *Geochem. J.* **29**, 91–95.
- Kenney J. and Keeping E. (1951) Mathematics of statistics, second ed., vol. 2. D. Van Nostrand Company, Inc., p. 162 (Chapter 7.11).
- Kollár D., Michel R. and Masarik J. (2006) Monte Carlo simulation of GCR neutron capture production of cosmogenic nuclides in stony meteorites and lunar surface. *Meteorit. Planet. Sci.* **41**, 375–389.
- Lee T., Papanastassiou D. A. and Wasserburg G. J. (1978) Calcium isotopic anomalies in the Allende meteorite. *Astrophys. J. Lett.* **220**, L21–L25.
- Lewis R. S., Ming T., Wacker J. F., Anders E. and Steel E. (1987) Interstellar diamonds in meteorites. *Nature* **326**, 160–162.
- Leya I., Schönbächler M., Wiechert U., Krähenbühl U. and Halliday A. N. (2008) Titanium isotopes and the radial heterogeneity of the Solar System. *Earth Planet. Sci. Lett.* **266**, 233–244.
- Leya I., Schönbächler M., Krähenbühl U. and Halliday A. N. (2009) New titanium isotope data for Allende and Efremovka CAIs. *Astrophys. J.* **702**, 1118–1126.
- Maréchal C. N., Télouk P. and Albarède F. (1999) Precise analysis of copper and zinc isotopic compositions by plasma-source mass spectrometry. *Chem. Geol.* **156**, 251–273.
- Masarik J. and Reedy R. C. (1994) Effects of bulk composition on nuclide production processes in meteorites. *Geochim. Cosmochim. Acta* **58**, 5307–5317.
- McCulloch M. T. and Wasserburg G. J. (1978a) Barium and neodymium isotopic anomalies in the Allende meteorite. *Astrophys. J. Lett.* **220**, L15–L19.
- McCulloch M. T. and Wasserburg G. J. (1978b) More anomalies from the Allende meteorite – samarium. *Geophys. Res. Lett.* **5**, 599–602.
- Mond L., Langer C. and Quincke F. (1890) Action of carbon monoxide on nickel. *J. Chem. Soc. Trans.* **57**, 749–753.
- Niederer F. R., Papanastassiou D. A. and Wasserburg G. J. (1980) Endemic isotopic anomalies in titanium. *Astrophys. J. Lett.* **240**, L73–L77.
- Niemeyer S. (1985) Systematics of Ti isotopes in carbonaceous chondrite whole-rock samples. *Geophys. Res. Lett.* **12**, 733–736.
- Niemeyer S. and Lugmair G. W. (1981) Ubiquitous isotopic anomalies in Ti from normal Allende inclusions. *Earth Planet. Sci. Lett.* **53**, 211–225.

- Niemeyer S. and Lugmair G. W. (1984) Titanium isotopic anomalies in meteorites. *Geochim. Cosmochim. Acta* **48**, 1401–1416.
- Nomoto K. (1982) Accreting white dwarf models for type I supernovae: I. Presupernova evolution and triggering mechanisms. *Astrophys. J.* **253**, 798–810.
- Nomoto K., Hashimoto M., Tsujimoto T., Thielemann F. K., Kishimoto N., Kubo Y. and Nakasato N. (1997) Nucleosynthesis in type II supernovae. *Nucl. Phys. A* **616**, 79–90.
- Papanastassiou D. A. and Wasserburg G. J. (1978) Strontium isotopic anomalies in the Allende meteorite. *Geophys. Res. Lett.* **5**, 595–598.
- Pelowitz D. B. (2005) MCNPX User's Manual Version 2.5.0. Los Alamos National Laboratory, Report LA-CP-05-0369 Edition.
- Qin L., Alexander C. M. O., Carlson R. W., Horan M. F. and Yokoyama T. (2010) Contributors to chromium isotope variation of meteorites. *Geochim. Cosmochim. Acta* **74**, 1122–1145.
- Quitté G., Markowski A., Latkoczy C., Gabriel A. and Pack A. (2010) Iron-60 heterogeneity and incomplete isotope mixing in the early Solar System. *Astrophys. J.* **720**, 1215–1224.
- Quitté G., Meier M., Latkoczy C., Halliday A. N. and Günther D. (2006) Nickel isotopes in iron meteorites – nucleosynthetic anomalies in sulphides with no effects in metals and no trace of  $^{60}\text{Fe}$ . *Earth Planet. Sci. Lett.* **242**, 16–25.
- Quitté G. and Oberli F. (2006) Quantitative extraction and high precision isotope measurements of nickel by MC-ICPMS. *J. Anal. Atom. Spectrom.* **21**, 1249–1255.
- Ranen M. C. and Jacobsen S. B. (2006) Barium isotopes in chondritic meteorites: implications for planetary reservoir models. *Science* **314**, 809–812.
- Rauscher T., Heger A., Hoffman R. D. and Woosley S. E. (2002) Nucleosynthesis in massive stars with improved nuclear and stellar physics. *Astrophys. J.* **576**, 323–348.
- Regelous M., Elliott T. and Coath C. D. (2008) Nickel isotope heterogeneity in the early Solar System. *Earth Planet. Sci. Lett.* **272**(1–2), 330–338.
- Reynolds J. H. and Turner G. (1964) Rare gases in the chondrite Renazzo. *J. Geophys. Res.* **69**, 3263–3281.
- Roberts-Austen W. C. (1898) The extraction of nickel from its ores by the Mond process. *Nature* **59**, 63–64.
- Rotaru M., Birck J. and Allègre C. (1992) Clues to early Solar System history from chromium isotopes in carbonaceous chondrites. *Nature* **358**, 465–470.
- Rugel G., Faestermann T., Knie K., Korschinek G., Poutivtsev M., Schumann D., Kivel N., Günther-Leopold I., Weinreich R. and Wohlmuther M. (2009) New measurement of the  $^{60}\text{Fe}$  half-life. *Phys. Rev. Lett.* **103**, 072502-1–072502-4.
- Russell W., Papanastassiou D. and Tombrello T. (1978) Ca isotope fractionation on the Earth and other Solar System materials. *Geochim. Cosmochim. Acta* **42**, 1075–1090.
- Steele R. C. J., Elliott T., Coath C. D., Regelous M. and Russell S. S. (2010) Correlated neutron-rich Ni isotope anomalies in chondritic and iron meteorites. *Lunar Planet. Sci.* **XLI** **41**, 1984.
- Strelow F. W. E., Victor A. H., Van Zyl C. R. and Eloff C. (1971) Distribution coefficients and cation exchange behavior of elements in hydrochloric acid–acetone. *Anal. Chem.* **43**, 870–876.
- Taylor P. D. P., Maeck R. and De Bièvre P. (1992) Determination of the absolute isotopic composition and atomic weight of a reference sample of natural iron. *Int. J. Mass Spectrom. Ion Process.* **121**, 111–125.
- Timmes F. X., Woosley S. E. and Weaver T. A. (1995) Galactic chemical evolution: hydrogen through zinc. *Astrophys. J. Suppl.* **98**, 617–658.
- Trinquier A., Birck J.-L. and Allègre C. J. (2007) Widespread  $^{54}\text{Cr}$  heterogeneity in the inner Solar System. *Astrophys. J.* **655**, 1179–1185.
- Trinquier A., Elliott T., Ulfbeck D., Coath C., Krot A. N. and Bizzarro M. (2009) Origin of nucleosynthetic isotope heterogeneity in the Solar protoplanetary disk. *Science* **324**, 374–376.
- Tschugaeff L. (1905) Ueber ein neues, empfindliches reagens auf nickel. *Ber. Deut. Chem. Ges.* **38**, 2520–2522.
- Vance D. and Thirlwall M. (2002) An assessment of mass discrimination in MC-ICPMS using Nd isotopes. *Chem. Geol.* **185**, 227–240.
- Victor A. H. (1986) Separation of nickel from other elements by cation-exchange chromatography in dimethylglyoxime/hydrochloric acid/acetone media. *Anal. Chim. Acta* **183**, 155–161.
- Voshage H. and Feldmann H. (1978) Investigations on cosmic-ray-produced nuclides in iron meteorites: 1. The measurement and interpretation of rare gas concentrations. *Earth Planet. Sci. Lett.* **39**, 25–36.
- Wahlgren M., Orlandini K. A. and Korkisch J. (1970) Specific cation-exchange separation of nickel. *Anal. Chim. Acta* **52**, 551–553.
- Wasserburg G. J., Lee T. and Papanastassiou D. A. (1977) Correlated O and Mg isotopic anomalies in Allende inclusions: II. Magnesium. *Geophys. Res. Lett.* **7**, 299–302.
- Weyer S. and Schwieters J. B. (2003) High precision Fe isotope measurements with high mass resolution MC-ICPMS. *Int. J. Mass Spectrom.* **226**, 355–368.
- Wombacher F. and Rehkämper M. (2003) Investigation of the mass discrimination of multiple collector ICP-MS using neodymium isotopes and the generalised power law. *J. Anal. Atom. Spectrom.* **18**, 1371–1375.
- Wombacher F., Rehkämper M. and Mezger K. (2004) Determination of the mass-dependence of cadmium isotope fractionation during evaporation. *Geochim. Cosmochim. Acta* **68**, 2349–2357.
- Woosley S. E. (1997) Neutron-rich nucleosynthesis in carbon deflagration supernovae. *Astrophys. J.* **476**, 801–810.
- York D. (1968) Least squares fitting of a straight line with correlated errors. *Earth Planet. Sci. Lett.* **5**, 320–324.
- Young E. D., Galy A. and Nagahara H. (2002) Kinetic and equilibrium mass-dependent isotope fractionation laws in nature and their geochemical and cosmochemical significance. *Geochim. Cosmochim. Acta* **66**, 1095–1104.

Associate editor: Dimitri A. Papanastassiou